*Journal of Sound and Vibration* (1997) **199**(1), 125–154

# SPECTRAL FINITE ELEMENT ANALYSIS OF THE VIBRATION OF STRAIGHT FLUID-FILLED PIPES WITH FLANGES

S. FINNVEDEN

*Institute of Sound and Vibration Research, University of Southampton, Southampton, SO17 1BJ, England*

(*Received* 17 *February* 1996, *and in final form* 21 *June* 1996)

A spectral finite element formulation for the analysis of stationary vibration of straight fluid-filled pipes is introduced. Element formulations for flanges and rigid masses attached to the pipe are also presented. In the spectral finite element formulation, the base functions are frequency-dependent solutions to the local equations of motion. The formulation is valid for arbitrarily long pipes and losses may be distributed in the system and may vary with frequency. The solutions of the equations of motion are expressed in terms of exponential functions, describing propagation in the waveguide, together with corresponding cross-sectional mode shapes. These solutions are found by using an FE discretization of the cross-sectional motion. To increase the numerical efficiency, methods for using FE shape functions with higher order polynomials are developed. The numerical accuracy is investigated by comparisons with results achieved with an exact formulation. It is found that, for frequencies of interest in many engineering problems, pipes may be modelled by using only one element to describe the fluid motion. The vibrations of a simple pipe structure with an infinite pipe, a flange and a small rigid mass are calculated. Just below the cut-on frequency of a shell mode, the stiffness controlled shell mode and the rigid mass may resonate, resulting in high vibration levels concentrated near the mass.



## 1. INTRODUCTION

Pipework systems in ships, oil and gas transport and processing industry form a very significant and vulnerable component of large scale critical systems. Vibrations in pipeworks often cause excessive noise radiation and may result in failure due to fatigue.

Predictions of vibrational response and vibration transmission in fluid-filled pipes by using the transfer matrix method have been made by Wang and Pinnington [1] and de Jong [2], both restricting the analysis to beam-type motion for the pipe walls. Frid [3], using a dynamic stiffness method and modal decomposition, calculated stationary and transient responses in fluid networks, while not considering the dynamics of the pipe wall. El-Raheb [4] calculated the resonances in finite length pipes, describing the cylinder motion with the "dry" modes, calculated with no fluid loading. Then, upon applying the kinematic coupling condition between cylinder and fluid, a transcendental eigenvalue problem for the fluid sound pressure was formulated. Apparently, this approach had limitations when formulating and assembling elements to describe structural motion [5]. Instead, the transfer matrices for pipe segments were formulated as in reference [4], with dry modes used for the cylinder, but with polynomial functions used to describe the axial dependence of the sound pressure [5]. The method is thus restricted to short pipe systems and comparatively low frequencies.

0022–460X/97/010125 + 30 $25.00/0/sv960602 

In this paper, a spectral finite element formulation is applied to straight fluid-filled pipes. This method [6–8], is a merger of the direct dynamic stiffness method (see, e.g., references [9–11]) and the finite element displacement method (see, e.g., reference [12]). Elements are formulated and assembled as in the standard FEM while the base functions are the frequency dependent local solutions of the equations of motion. Compared with the standard FEM, this allows a reduction of the number of d.o.f., while increasing accuracy. The FE formalism increases the applicability of the dynamic stiffness method since standard FE approximations can be incorporated. Moreover, the routines for calculating the dynamic stiffness matrices when base functions are exponential functions, originally developed in reference [7], reduces the efforts in the element formulation considerably.

The solutions of the equations of motion (that is, for the waves in a fluid-filled pipe) were originally investigated by Fuller and Fahy [13]. Their approach, namely solving the characteristic equation, once the sound pressure is expressed as a linear function of the radial displacement, results in a non-linear, transcendental, eigenvalue problem, which is non-trivial to handle. Pavic [14], deriving expressions for the power flow in pipes, reduced this eigenvalue problem to non-linear algebraic form, by employing a series expansion of the Bessel functions describing the sound pressure.

In prismatic waveguide structures, as e.g., pipes, the solutions of the equations of motion are expressed by using exponential terms, which describe the propagation in the axial direction, together with corresponding cross-sectional mode shapes. As originally proposed by Gavric [15], and in a slightly different form by Etouney *et. al*. [16], the cross-sectional mode shapes may be described with standard linear FE shape functions. Upon applying such a description, the equations of motion take the form of a set of coupled ODE's with constant coefficients. Thus, the solutions of these equations are exponential functions. Upon assuming this, and applying the transformations used by Gavric [15] (or the slightly improved version in reference [17]), a standard linear eigenvalue problem results.

When applying a Fourier decomposition of the angular dependence of the displacements of fluid-filled pipes, the cross-sectional mode shapes are given by the relative amplitudes of the radial, axial and tangential cylinder displacements and the radial dependence of the sound pressure in the fluid. When applying the FE technique, by discretizing the sound pressure in cylindrical segments, the dispersion relations are found by standard linear matrix operations, with considerably higher efficiency than the methods in references [13] and [4]. The robustness of the FE method, and of standard linear algebra, suggests that the proposed method is suitable not only for research but also for engineering application.

Standard linear shape functions are, however, not fully efficient in describing the fluid motion. ''The requirement that the mesh of elements in the fluid be sufficiently fine to capture the sharp radial gradients of pressure near the wall is a source of considerable burden of computation'' [5]. To overcome this, a variant of the p-version of the FE method [18], or perhaps a variant of the hierarchical FE method (see, e.g., reference [19]), is applied. That is, the shape functions used are polynomials of higher order, this leading to a tremendous increase in accuracy achieved with a given number of d.o.f.. A versatile method is developed to calculate suitable sets of higher order shape functions and the corresponding dynamic stiffness matrices.

In section 2, the equations governing the coupled motion of a thin-walled cylinder and a viscous fluid are formulated, as well as those for flanges. In section 3 the dispersion relations for straight fluid-filled pipes, are found by using the FE method. The accuracy of the method is estimated by comparisons with results achieved with the exact formulation by Fuller and Fahy [13]. In section 4, the spectral finite element formulation for arbitrarily long pipes is presented together with formulations for flanges and rigid masses attached

to cylinders. Finally, in section 5, a small calculation example is given as a demonstration of the kind of problems that may be investigated within minutes on a PC. This example also reveals a possible mechanism for fatigue in thin-walled pipe structures.

## 2. GOVERNING EQUATIONS

The functionals, similar to those used in the method of virtual work, governing the motion of a cylindrical pipe with a contained viscous fluid are formulated. The corresponding functional describing an attached flange's motion is also derived. The equations are formulated in the frequency domain with a time dependence, $e^{-i\omega t}$, implicitly assumed. Dissipative losses, possibly frequency dependant are, for each structural component, assumed proportional to either its inertia or its stiffness. That is, the equations below apply equally when

$$E = E_0(1 - i\eta_e), \qquad G = G_0(1 - i\eta_s), \qquad \rho = \rho_0(1 + i\eta_v), \tag{1}$$

where $E$ is Young's modulus, $G$ is the shear modulus, $\rho$ is the density and $\eta_e$, $\eta_s$, $\eta_v$ are loss factors.

As shown in reference [7], these losses may be accounted for by employing a variational principle similar to that of Hamilton whereby, in the functionals describing kinetic and potential energies, the quadratic forms in the displacements are replaced with symmetric bi-linear forms in the displacements and in the complex conjugates of the displacements in an adjoint negatively damped system [20, 21]. While conceptually slightly more complex, this approach does not require any extra calculation effort. With this approach, the machinery of variational methods is also retained for non-conservative systems. Thus, it is possible to formulate the energies in whatever co-ordinate system is appropriate or convenient, to use Lagrange multipliers to impose restraints on motion, and to formulate the equations of motion without having to express forces explicitly, these requiring a more complex description than the displacements. Finally, by using a Rayleigh-Ritz procedure to formulate the equations of motion, it is possible to choose the variational parameters at will. Hence, the trial functions could be exact solutions to the local equations of motions, as in reference [7], or approximate solutions, as in reference [8], or, as in this work, a mixture of exact solutions and FE polynomial approximations.

### 2.1. CYLINDER FORMULATION

The Arnold and Warburton theory for vibrations of cylinders is beautifully presented in the original work [22], but for the sake of self-consistency it is recapitulated here. Also, most of the intermediate expressions are needed for the element formulations in sections 3 and 4.

As shown in Figure 1, a thin walled cylinder is considered for which the strains

$$e_z = \gamma_{zx} = \gamma_{z\phi} = 0. \tag{2}$$

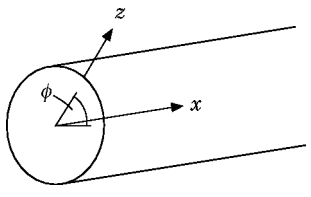


Figure 1. Cylinder co-ordinate system.

Hence, with the trapezoidal form of a cylinder segment neglected, an analogy to strain energy, $e_p$, is

$$e_p = E' \int \mathrm{d}x \int_0^{2\pi} R \, \mathrm{d}\phi \int_{-T_c/2}^{T_c/2} \mathrm{d}z[e_x^a e_x + e_\phi^a e_\phi + v(e_x^a e_\phi + e_\phi^a e_x) + g\gamma_{x\phi}^a \gamma_{x\phi}], \tag{3}$$

where $R$ is the cylinder radius, $T_c$ is the shell thickness, $E' = E/(1 - v^2)$, $g = G/E'$, $v$ is Poisson's ratio and the superscript $a$ denotes the complex conjugate of the corresponding strain in the adjoint system.

The Kirchhoff hypothesis is adopted and a trigonometric dependence of $\phi$ is assumed for the displacements:

$$u_x = (u + z\theta_1)\cos(n\phi), \qquad u_\phi = (v + z\theta_2)\sin(n\phi), \qquad u_z = w\cos(n\phi), \tag{4a}$$

in which, from equations (2),

$$\theta_1 = -\partial w/\partial x, \qquad \theta_2 = (v + nw)/R. \tag{4b}$$

Upon using these displacements, while neglecting all but the dominating terms in $z/R$, the strains are given by [22]

$$e_x = (\varepsilon_x + z\kappa_1)\cos(n\phi), \qquad e_\phi = (\varepsilon_\phi + z\kappa_2)\cos(n\phi), \qquad \gamma_{x\phi} = (\gamma + z\tau)\sin(n\phi), \tag{5}$$

where

$$\varepsilon_x = \partial u/\partial x, \qquad \varepsilon_\phi = (nv + w)/R, \qquad \gamma = -(nu/R) + \partial v/\partial x,$$
$$\kappa_1 = -\partial^2 w/\partial x^2, \qquad \kappa_2 = (nv + n^2 w)/R^2, \qquad \tau = (2/R)(\partial v/\partial x + n\,\partial w/\partial x). \tag{6}$$

The same relations apply between the complex conjugates of strains and displacements in the adjoint system. Thus, upon carrying out the integration over $z$ and $\phi$, the functional $L_{cyl}$, which is stationary for true motion of the cylinder, is found to be

$$L_{cyl} = \int (e_p - e_k)\,\mathrm{d}x^3 = E' T_c R \Lambda_n \int \mathrm{d}x[\varepsilon_x^a \varepsilon_x + \varepsilon_\phi^a \varepsilon_\phi + v(\varepsilon_x^a \varepsilon_\phi + \varepsilon_\phi^a \varepsilon_x) + g\gamma^a \gamma$$
$$+ (T_c^2/12)(\kappa_1^a \kappa_1 + \kappa_2^a \kappa_2 + v(\kappa_1^a \kappa_2 + \kappa_2^a \kappa_1) + g\tau^a \tau) - \omega^2/c_L^2 (u^a u + v^a v + w^a w)], \tag{7}$$

where $e_k$ is the analogy to kinetic energy density and where

$$c_L^2 = E'/\rho, \qquad \Lambda_n = 2\pi \quad \text{for } n = 0, \qquad \Lambda_n = \pi \quad \text{for } n \geqslant 1. \tag{8}$$

Thus, requiring $L_{cyl}$ to be stationary is equivalent to requiring the displacements to be solutions of the equations of motion (see, e.g., equation 2.9b of reference [23]).

### 2.2. FORMULATION FOR FLANGES

The flanges, see Figure 2, are considered as flat circular annuli outstands with thickness, $T_f$, having outer radius $r = R_0$ and joined to the cylinder at $r = R_i$. Upon adopting the Kirchhoff hypothesis the out-of-plane strains are

$$e_x = \gamma_{xr} = \gamma_{x\phi} = 0, \tag{9}$$

and upon assuming a trigonometric dependence on $\phi$, compatible with that for the cylinder, the displacements and the in-plane strains are

$$u_r = (u - x\,\partial w/\partial r)\cos(n\phi), \qquad u_\phi = (v + xnw/r)\sin(n\phi), \qquad u_x = w\cos(n\phi), \tag{10}$$

$$e_r = (\varepsilon_r - x\kappa_1)\cos(n\phi), \qquad e_\phi = (\varepsilon_\phi - x\kappa_2)\cos(n\phi), \qquad \gamma_{x\phi} = (\gamma - x\tau)\sin(n\phi), \tag{11}$$

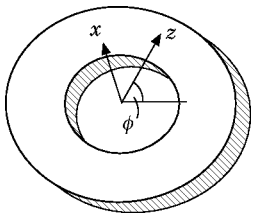


Figure 2. Flange co-ordinate system.

where

$$\varepsilon_r = \partial u/\partial r, \qquad \varepsilon_\phi = (u + nv)/r, \qquad \gamma = -(nu + v)/r + \partial v/\partial r,$$

$$\kappa_1 = \partial^2 w/\partial r^2, \qquad \kappa_2 = (1/r)\partial w/\partial r - n^2 w/r^2, \qquad \tau = (2n/r)[(w/r) - \partial w/\partial r]. \tag{12}$$

Inserting these expressions, and the corresponding ones for the adjoint system, into the functional governing the virtual work, $L_{fla}$, and carrying out the $\phi$ and $x$ integrals, results in

$$L_{fla} = E' T_f \Lambda_n \int_{R_i}^{R_0} r \, \mathrm{d}r[\varepsilon_r^a \varepsilon_r + \varepsilon_\phi^a \varepsilon_\phi + \nu(\varepsilon_r^a \varepsilon_\phi + \varepsilon_\phi^a \varepsilon_r) + g\gamma^a\gamma$$

$$+ (T_f^2/12)(\kappa_1^a\kappa_1 + \kappa_2^a\kappa_2 + \nu(\kappa_1^a\kappa_2 + \kappa_2^a\kappa_1) + g\tau^a\tau) - \omega^2/c_L^2(u^a u + v^a v + w^a w)]. \tag{13}$$

### 2.3. VISCOUS FLUID WITH COUPLING CONDITION TO CYLINDER

In the absence of sources, for a time dependence $\mathrm{e}^{-\mathrm{i}\omega t}$, the acoustic motion of a viscous fluid is determined by [24, p. 15]

$$-\mathrm{i}\omega\delta + \rho_f \,\mathrm{div}\,(\mathbf{u}) = 0, \qquad -\mathrm{i}\rho_f\omega(1 + \mathrm{i}\eta_v)\mathbf{u} = -\nabla p, \qquad \delta = p/c^2(1 - \mathrm{i}\eta_e), \tag{14}$$

where $p$ is the sound pressure, $\mathbf{u}$ is the particle velocity, $\delta$ is the acoustic perturbation of the density, $\rho_f$ is the density, $c$ is the sound speed and $\eta_v$ and $\eta_e$ are loss factors, possibly frequency dependent, as discussed in reference [7]. Examples of such loss factors are found in reference [25, see p. 254 and p. 283]. The equation of motion for this fluid is

$$\nabla^2 p + (\omega^2/c^2)[(1 + \mathrm{i}\eta_v)/(1 - \mathrm{i}\eta_e)]p = 0 \tag{15}$$

Consider now an adjoint, negatively damped, system described by

$$-\mathrm{i}\omega\delta^A + \rho_f \,\mathrm{div}\,(\mathbf{u}^A) = 0, \qquad -\mathrm{i}\rho_f\omega(1 - \mathrm{i}\eta_v)\mathbf{u}^A = -\nabla p^A, \qquad \delta^A = p^A/c^2(1 + \mathrm{i}\eta_e), \tag{16}$$

$$\nabla^2 p^A + (\omega^2/c^2)[(1 - \mathrm{i}\eta_v)][(1 + \mathrm{i}\eta_e)]p^A = 0. \tag{17}$$

The complex conjugate of the sound pressure in the adjoint system, i.e. $p^a = (p^A)^*$ is a solution to:

$$\nabla^2 p^a + (\omega^2/c^2)[(1 + \mathrm{i}\eta_v)/(1 - \mathrm{i}\eta_e)]p^a = 0. \tag{18}$$

That is, the same equation applies to $p$ and $p^a$. The functional $L_f$ is defined, in analogy with the Lagrangian, so that $L_f$ is stationary for the solutions of equations (15) and (18). Hence, requiring that

$$\delta L_f = 0, \tag{19}$$

is equivalent to equations (15) and (18), if $L_f$ is given by

$$L_f = C \int \mathrm{d}x^3 \left[ \nabla p^a \nabla p - \frac{\omega^2}{c^2} \frac{1 + \mathrm{i}\eta_v}{1 - \mathrm{i}\eta_e} p^a p \right]. \tag{20}$$

$C$ is an arbitrary constant, which will be determined so that $L_f$ expresses the analogy of the virtual work. Now, the kinematic coupling condition between fluid and structure is

$$-\mathrm{i}\omega w = \mathbf{nu}, \tag{21}$$

where $\mathbf{n}$ is the unit vector, in the direction of the outward pointing normal to the fluid domain. The work done by the fluid when the structure is displaced an amount $w$, in the direction, $\mathbf{n}$, is

$$B_{fc} = \int p^a w + p w^a \, \mathrm{d}x^2. \tag{22}$$

This work is evidently equal to minus the work on the fluid. In the absence of sources, $B_{fc}$ is therefore equal to minus the "virtual work " in the fluid, so that the functional $L_f + B_{fc}$ should be stationary. Upon taking the variation of $p^a$, one has

$$\int \delta p^a [C\mathbf{n}\nabla p + w] \, \mathrm{d}x^2 - C \int \delta p^a \left[ \nabla^2 p + \frac{\omega^2}{c^2} \frac{1 + \mathrm{i}\eta_v}{1 - \mathrm{i}\eta_e} p \right] \mathrm{d}x^3 = 0. \tag{23}$$

Hence, upon using equation (14b), equation (21) is satisfied if

$$C = -1/\rho_f \omega^2 (1 + \mathrm{i}\eta_v). \tag{24}$$

In analogy to the standard acoustic velocity potential [25], to obtain a resulting functional with a frequency dependence similar to that in the structure's functional and a dependence on $\phi$ compatible with that of the cylinder, the velocity potentials $\psi$ and $\psi^a$ are introduced:

$$p = \rho_f \omega \cos(n\phi)\psi, \qquad p^a = p_f \omega \cos(n\phi)\psi^a. \tag{25}$$

Thus, the functionals $L_f$ and $B_{fc}$ are

$$L_f = -\Lambda_n \frac{\rho_f}{1 + \mathrm{i}\eta_v} \int \left[ \left( \frac{\partial \psi^a}{\partial x} \frac{\partial \psi}{\partial x} + \frac{\partial \psi^a}{\partial r} \frac{\partial \psi}{\partial r} + \frac{n^2}{r^2} \psi^a \psi \right) - \frac{\omega^2 (1 + \mathrm{i}\eta_v)}{c^2 (1 - \mathrm{i}\eta_e)} \psi^a \psi \right] r \, \mathrm{d}r \, \mathrm{d}x, \tag{26}$$

$$B_{fc} = \Lambda_n R \int \rho_f \omega [\psi^a w + \psi w^a] \, \mathrm{d}x. \tag{27}$$

This expression differs by a factor $1/(1 + \mathrm{i}\eta_v)$ from the corresponding expression for the "Lagrange density" given by Morse and Ingard [25, equation 6.2.28]. In this way, the functional expresses an analogy to the virtual work and may directly be used together with the corresponding functionals for the structure. That is, subtracting $L_f + B_{fc}$ from the functional describing the pipe vibration, $L_{cyl}$, equation (7), produces a functional

$$L = L_{cyl} - L_f - B_{fc}, \tag{28}$$

which is stationary for true motion. This means that requiring $\delta L = 0$ is equivalent to finding a solution to the equations of motion for the fluid (15), the kinematic coupling condition ( 21) and the equations of motion for the cylinder [23, equation (2.9b)], as can be verified by direct calculations.

## 3. DISPERSION RELATIONS

The possible waves in a fluid filled pipe are found, expressed by exponential terms determining the propagation along the pipe, together with corresponding cross-sectional mode shapes. As a circular dependence on $\phi$ is already assumed, these mode shapes are given by the relative amplitudes of the cylinder displacement and by the radial dependence of the fluid velocity potential, here approximated by polynomials. First, a standard FE approximation with piece-wise linear functions within cylinder segments is used. To improve efficiency, higher order polynomial approximations are also derived, providing a tremendous increase in accuracy for a given number of d.o.f.. With polynomial trial functions, the cross-sectional motion is expressed as an explicit function of nodal displacements. Upon inserting these functions into the functional $L$, equation (28), the resulting Euler-Lagrange equations are a set of coupled ODE's which, as in reference [17], are transformed to a standard linear eigenvalue problem.

### 3.1. ROUTINES FOR THE INTEGRATION OF DYNAMIC STIFFNESS MATRICES

A set of subroutines was developed to manipulate polynomial functions so that the dynamic stiffness matrices are easily and systematically calculated. As these may be of common interest they are here presented in a general form, while being directly applicable to any of the elements presented.

Consider one trial function, $u(x)$, used in a 1-D FE formulation;

$$u(x) = \mathbf{P}_u * \mathbf{B}_u * \mathbf{W}, \tag{29}$$

where the column vector $\mathbf{W}$ contains the variational parameters, usually the nodal d.o.f., the row – vector $\mathbf{P}_u$ is

$$\mathbf{P}_u(x) = [a_1 x^{n_1} \quad a_2 x^{n_2} \cdots a_m x^{n_m}], \tag{30}$$

and the m * m matrix $\mathbf{B}_u$ projects $\mathbf{P}_u$ onto the nodal d.o.f.. For instance, the trial function used for a standard Euler-Bernoulli beam of length $2l$ is defined by

$$\mathbf{P}_u = [1 \quad x/l \quad (x/l)^2 \quad (x/l)^3], \qquad \mathbf{W} = [u(-l) \quad \partial u(-l)/\partial x \quad u(l) \quad \partial u(l)/\partial x]^T, \tag{31}$$

while the columns of the matrix $\mathbf{B}_u$ contain the coefficients of the first order Hermitian shape functions [12, equation (3.125)].

To manipulate easily trial functions of the form (29), the coefficients of $\mathbf{P}_u$ are stored in the 2 * m matrix $\mathbf{U}$,

$$\mathbf{U} = \begin{bmatrix} \mathbf{A}_u \\ \mathbf{N}_u \end{bmatrix} = \begin{bmatrix} a_1 & a_2 & \cdots & a_m \\ n_1 & n_2 & \cdots & n_m \end{bmatrix}, \tag{32}$$

so that operating on $\mathbf{P}_u$ is represented by functions with $\mathbf{U}$ as the argument. Similarly a polynomial $\mathbf{P}_v$ will be represented by a matrix $\mathbf{V}$.

The routines below are presented by using the array operators "dot product", "dot power" and "dot division", all as implemented in the Matlab code.

#### 3.1.1. *Evaluating the elements of* $\mathbf{P}_u$

$$\mathrm{Ev}(\mathbf{U}, c) = \mathbf{P}_u(x = c) = \mathbf{A}_u \,.*\, (c \,.\hat{}\, \mathbf{N}_u). \tag{33}$$

3.1.2. *Differentiating* $\mathbf{P}_u$

If $\mathbf{P}_v = \partial \mathbf{P}_u / \partial x$, then

$$\mathbf{V} = \mathrm{Dif}\,(\mathbf{U}) = \begin{bmatrix} \mathbf{A}_u * \mathbf{N}_u \\ \mathbf{N}_u - 1 \end{bmatrix}. \tag{34a}$$

Define

$$\mathrm{Dif}\,(\mathbf{U}, 2) = \mathrm{Dif}\,(\mathrm{Dif}\,(\mathbf{U})). \tag{34b}$$

3.1.3. *Integrate the outer product of* $\mathbf{P}_u$ and $\mathbf{P}_v$

Define the matrix generating function

$$\mathrm{Int}\,(\mathbf{U}, \mathbf{V}, \mathbf{L}) = \int_{\mathbf{L}[1]}^{\mathbf{L}[2]} [\mathbf{P}_u]^{\mathrm{T}} * \mathbf{P}_v \, \mathrm{d}x,$$

and define the matrix $\mathbf{Q}$ with elements

$$\mathbf{Q}[i, j] = \mathbf{N}_u[i] + \mathbf{N}_v[j] + 1; \tag{35a}$$

then

$$\mathrm{Int}\,(\mathbf{U}, \mathbf{V}, \mathbf{L}) = [[\mathbf{A}_u]^{\mathrm{T}} * \mathbf{A}_v] \cdot{*} [\mathbf{L}[2] \cdot{\wedge} \mathbf{Q} - \mathbf{L}[1] \cdot{\wedge} \mathbf{Q}] \cdot{/} \mathbf{Q}. \tag{35b}$$

Similarly

$$\mathrm{Intr}\,(\mathbf{U}, \mathbf{V}, \mathbf{L}) = \int_{\mathbf{L}[1]}^{\mathbf{L}[2]} [\mathbf{P}_u]^{\mathrm{T}} * \mathbf{P}_v x \, \mathrm{d}x, \qquad \mathbf{Qr}[i, j] = \mathbf{N}_u[i] + \mathbf{N}_v[j] + 2, \tag{36a}$$

$$\mathrm{Intr}\,(\mathbf{U}, \mathbf{V}, \mathbf{L}) = [[\mathbf{A}_u]^{\mathrm{T}} * \mathbf{A}_v] \cdot{*} [\mathbf{L}[2] \cdot{\wedge} \mathbf{Qr} - \mathbf{L}[1] \cdot{\wedge} \mathbf{Qr}] \cdot{/} \mathbf{Qr}, \tag{36b}$$

with the exception for those elements in $\mathbf{Qr}$ which are zero. If element $[i, j]$ of the matrix $\mathbf{Qr}$ is zero then the $[i, j]$ element of $\mathbf{P} = \mathrm{Intr}\,(\mathbf{U}, \mathbf{V}, \mathbf{L})$ is

$$\mathbf{P}[i, j] = \mathbf{A}_u[i] * \mathbf{A}_v[j] * (\mathrm{Ln}\,(\mathbf{L}[2]) - \mathrm{Ln}\,(\mathbf{L}[1])), \tag{36c}$$

provided that $x = 0$ is not in the integration range. Define

$$\mathrm{Int}\,(\mathbf{V}, \mathbf{L}) = \mathrm{Int}\,(\mathbf{V}, \mathbf{V}, \mathbf{L}), \qquad \mathrm{Intr}\,(\mathbf{V}, \mathbf{L}) = \mathrm{Intr}\,(\mathbf{V}, \mathbf{V}, \mathbf{L}). \tag{37}$$

3.1.4. *Multiplication with a one-term polynomial*

If $\mathbf{P}_w = \mathbf{P}_u * \mathbf{P}_v$, where $\mathbf{P}_v = \mathbf{V}(1) * x^{\mathbf{V}(2)}$, then

$$\mathbf{W} = \mathrm{Mul}(\mathbf{U}, \mathbf{V}) = \begin{bmatrix} \mathbf{A}_u * \mathbf{V}(1) \\ \mathbf{N}_u + \mathbf{V}(2) \end{bmatrix}. \tag{38}$$

3.1.5. *Adding two polynomials*

If $\mathbf{P}_w = \mathbf{P}_u + \mathbf{P}_v$, then

$$\mathbf{W} = \mathrm{Add}\,(\mathbf{U}, \mathbf{V}) = \begin{bmatrix} \mathbf{A}_u + \mathbf{A}_v \\ \mathbf{N}_u \end{bmatrix}, \tag{39}$$

provided that $\mathbf{N}_u = \mathbf{N}_v$.

3.1.6. *Example*

Upon using these routines for the Euler-Bernoulli beam then $\mathbf{B_u}$, if not known, is

$$\mathbf{B_u} = \begin{bmatrix} \text{Ev}\,(\mathbf{U}, -l) \\ \text{Ev}\,(\text{Dif}\,(\mathbf{U}), -l) \\ \text{Ev}\,(\mathbf{U}, l) \\ \text{Ev}\,(\text{Dif}\,(\mathbf{U}), l) \end{bmatrix}^{-1}. \tag{40}$$

The Lagrangian is

$$L = \int_{\text{L(1)}}^{\text{L(2)}} (B(\partial^2 u/\partial x^2)^2 - \omega^2 m(u)^2)\,\mathrm{d}x = \mathbf{W}^{\mathrm{T}} * \mathbf{Lag} * \mathbf{W}, \tag{41}$$

where $\mathbf{L} = [-l \quad l]$, $B$ is the bending rigidity, $m$ is the mass per unit length and the dynamic stiffness matrix **Lag** is

$$\mathbf{Lag} = [\mathbf{B_u}]^{\mathrm{T}} * [B\ \text{Int}\,(\text{Dif}\,(\mathbf{U}, 2), \mathbf{L}) - \omega^2 m\ \text{Int}\,(\mathbf{U}, \mathbf{L})] * \mathbf{B_u}. \tag{42}$$

To sum up, giving the Lagrangian, the nodal d.o.f. and the degree of the polynomial to use, the dynamic stiffness matrix is evaluated with three lines of command: (32), (40) and (42).

## 3.2. ASSEMBLY OF THE DISPERSION RELATIONS

3.2.1. *Fluid*

As originally proposed by Gavric [15], the cross-sectional mode shapes in a prismatic wave guide are approximated with standard FE shape functions. Thus, the fluid domain is divided into cylindrical segments in which the velocity potential, equation (25), is

$$\psi(r, x) = \mathbf{P_f}(\mathrm{r}) * \mathbf{B_f} * \Psi(x), \tag{43}$$

where, for an element defined in a segment, $R_i \leqslant r \leqslant R_o$, with piece-wise linear shape functions,

$$\mathbf{P_f} = [1 \quad r/R_i], \qquad \mathbf{B_f} = \frac{1}{R_o/R_i - 1}\begin{bmatrix} R_i/R_o & -1 \\ -1 & 1 \end{bmatrix}, \qquad \Psi = [\psi(R_i, x) \quad \psi(R_o, x)]^{\mathrm{T}}. \tag{44}$$

Similarly, for the adjoint system

$$\psi^a(r, x) = \mathbf{P_f} * \mathbf{B_f} * \Psi^a. \tag{45}$$

Now, define $\mathbf{R} = [R_i\ R_o]$ and, as in Section 3.1, represent the polynomials $\mathbf{P_f}$ and $n/r\ \mathbf{P_f}$ with the matrices $\mathbf{U_0}$ and $\mathbf{U_1}$:

$$\mathbf{U_0} = \begin{bmatrix} 1 & 1/R_i \\ 0 & 1 \end{bmatrix}, \qquad \mathbf{U_1} = \begin{bmatrix} n & n/R_i \\ -1 & 0 \end{bmatrix}. \tag{46}$$

Then, the functional $L_f$, equation (26), is

$$L_f = -[\Psi^a]^{\mathrm{T}} * [\mathbf{k_0} - \omega^2 \mathbf{m}] * [\Psi] - [\partial\Psi^a/\partial x]^{\mathrm{T}} * [\mathbf{k_2}] * [\partial\Psi/\partial x], \tag{47}$$

where

$$\mathbf{k_0} = \Lambda_n \frac{\rho_f}{1 + \mathrm{i}\eta_v}\,\mathbf{B}_f^{\mathrm{T}} * [\text{Intr}\,(\text{Dif}\,(\mathbf{U_0}), \mathbf{R}) + \text{Intr}\,(\mathbf{U_1}, \mathbf{R})] * \mathbf{B_f}, \tag{48a}$$

$$\mathbf{m} = \Lambda_n \frac{\rho_f}{c^2(1 - i\eta_e)} \mathbf{B}_f^{\mathrm{T}} * [\mathrm{Intr}\,(\mathbf{U_0}, \mathbf{R})] * \mathbf{B_f}, \qquad \mathbf{k_2} = \Lambda_n \frac{\rho_f}{1 + i\eta_v} \mathbf{B}_f^{T} * [\mathrm{Intr}\,(\mathbf{U_0}, \mathbf{R})] * \mathbf{B_f}. \tag{48b, c}$$

These matrices may be assembled into global matrices $\mathbf{K_0}$, $\mathbf{K_2}$ and $\mathbf{M}$.

If $r = 0$ is within the elements' domain and if $n \geqslant 1$, the shape function must be modified since, as the functional must remain finite, the constant velocity potential is not an admissible function in this case. Instead, the trial function is as in equation (29), with

$$\mathbf{P_f} = [r/R_o \quad (r/R_o)^2], \qquad \mathbf{B_f} = \begin{bmatrix} 1 & 0 \\ -1 & 1 \end{bmatrix}, \qquad \Psi = \begin{bmatrix} R_o \dfrac{\partial \psi(0)}{\partial r} & \psi(R_o) \end{bmatrix}^{\mathrm{T}}, \tag{49}$$

whereas the matrices $\mathbf{U_0}$ and $\mathbf{U_1}$ are changed accordingly. With these definitions, the rest of the calculations, i.e., equations (47) and (48), remains unchanged.

### 3.2.2. *Coupling conditions*

The coupling of fluid and cylinder is, as in equation (28), accounted for by the functional $B_{fc}$ which is expressed as

$$B_{fc} = \omega[w^a \quad [\Psi^a]^{\mathrm{T}}] * \begin{bmatrix} 0 & \mathbf{C} \\ \mathbf{C}^{\mathrm{T}} & 0 \end{bmatrix} * \begin{bmatrix} w \\ \Psi \end{bmatrix}, \qquad \mathbf{C} = \Lambda_n R \rho_f \,\mathrm{Ev}\,(\mathbf{U_0}, R) * \mathbf{B_f}. \tag{50}$$

### 3.2.3. *Higher order polynomial shape functions*

To increase the efficacy of the FE method in calculating cross-sectional mode shapes and wavenumbers, a higher order polynomial approximation is attempted. For the one-dimensional elements used, approximating the solution to a second order equation, there are only two boundary conditions to satisfy. Hence, the additional d.o.f.'s must be specified by other means. Often (see, e.g., references [12, section 3.8] and [18, section 8.7]), extra d.o.f.'s are specified as the functions' values at interior nodes. This approach, however, leads to rather complex algebra and appears to apply unnecessary constraints; since variational parameters can be chosen at will, they need not be nodal displacements.

Now, consider a trial function of polynomial form

$$u(x) = \mathbf{F}(x) * \begin{bmatrix} \mathbf{W} \\ \mathbf{W_{int}} \end{bmatrix}, \tag{51}$$

where $\mathbf{W}$ contains $m$ nodal d.o.f.'s, $\mathbf{W_{int}}$ are $n$-$m$ internal d.o.f.'s and where

$$\mathbf{F} = [1 \quad x \quad \cdots \quad x^{n-1}] * \mathbf{a} = \mathbf{f}(x) * \mathbf{a}. \tag{52}$$

The n $*$ n matrix $\mathbf{a}$ is to be determined so that the boundary conditions, which $u$ should satisfy, depend solely on $\mathbf{W}$, with the coupling of the element to other elements being independent of $\mathbf{W_{int}}$.

The boundary conditions which $u$ and hence $\mathbf{F}$, should obey are, for instance, of the form

$$u(x_1) = \mathbf{W}[1], \qquad u(x_2) = \mathbf{W}[2], \qquad \partial u/\partial x(x_1) = \mathbf{W}[3], \ldots .$$

These conditions are, in matrix form,

$$\mathbf{A} * \mathbf{a} * \begin{bmatrix} \mathbf{W} \\ \mathbf{W}_{\text{int}} \end{bmatrix} = \begin{bmatrix} \text{Ev}\,(\mathbf{f}, x_1) \\ \text{Ev}\,(\mathbf{f}, x_2) \\ \text{Ev}\,(\text{Dif}\,(\mathbf{f}), x_1) \\ \vdots \end{bmatrix} * \mathbf{a} * \begin{bmatrix} \mathbf{W} \\ \mathbf{W}_{\text{int}} \end{bmatrix} = [\mathbf{I} \quad \mathbf{O}] * \begin{bmatrix} \mathbf{W} \\ \mathbf{W}_{\text{int}} \end{bmatrix}. \tag{53}$$

As these conditions should apply for all $\mathbf{W}$ and $\mathbf{W}_{\text{int}}$ and the dimension of the matrix $\mathbf{A}$ is $m * n$, there are $m * n$ conditions for the $n * n$ unknown elements of $\mathbf{a}$. To find a solution of this under-determined equation system, apply a singular value decomposition of $\mathbf{A}$ [26, section 5.2.5],

$$\mathbf{A} = \mathbf{Q}_2 \Sigma [\mathbf{Q}_1]^T, \qquad \Sigma = [\Sigma_1 \quad \mathbf{0}], \tag{54}$$

where $\Sigma_1$ is a $m * m$ diagonal matrix and $\mathbf{0}$ is an $m * (n–m)$ matrix of zeros. $\mathbf{Q}_1$ and $\mathbf{Q}_2$ are orthogonal matrices of size $n * n$ and $m * m$. On this basis, define

$$\mathbf{a} = \mathbf{Q}_1 \mathbf{b}. \tag{55}$$

Then the boundary conditions (53) are, with $\mathbf{b}$ in partitioned form,

$$\mathbf{A} * \mathbf{a} = \mathbf{Q}_2 [\Sigma_1 \quad \mathbf{0}] \begin{bmatrix} \mathbf{b}_{1.1} & \mathbf{b}_{1.2} \\ \mathbf{b}_{2.1} & \mathbf{b}_{2.2} \end{bmatrix} = [\mathbf{I} \quad \mathbf{0}]. \tag{56}$$

This equation implies nothing about submatrices $\mathbf{b}_{2.1}$ and $\mathbf{b}_{2.2}$, while from it $\mathbf{b}_{1.2}$ is determined as a matrix of zeros and $\mathbf{b}_{1.1}$ as

$$\mathbf{b}_{1.1} = [\Sigma_1]^{-1} [\mathbf{Q}_2]^{\text{T}}. \tag{57}$$

Finally, one may chose $\mathbf{b}_{2.2}$ as an identity matrix and $\mathbf{b}_{2.1}$ as a matrix of zeros, thus ensuring that the internal d.o.f. $\mathbf{W}_{\text{int}}$ projects onto displacements which on the boundary are linearly independent and which are in the null space of $\mathbf{A}$, hence not influencing the coupling to other elements. To sum up, a trial function $u$, of polynomial order $n$, which obeys $m$ boundary conditions, $m < n$, is

$$u(x) = \mathbf{f}(x) \mathbf{Q}_1 \begin{bmatrix} [\Sigma_1]^{-1} [\mathbf{Q}_2]^{\text{T}} & \mathbf{0} \\ \mathbf{0} & \mathbf{I} \end{bmatrix} \begin{bmatrix} \mathbf{W} \\ \mathbf{W}_{\text{int}} \end{bmatrix}. \tag{58}$$

This quite simple expression is of the form (29), so that the routines defined in Section 3.1 could be applied to calculate the dynamic stiffness matrix for the element. For the fluid element, with trial function defined in equation (43), one may identify $\mathbf{P}_{\text{f}} = \mathbf{f}$, so that the boundary conditions are governed by $\mathbf{A}$:

$$\mathbf{A} = \begin{bmatrix} \text{Ev}\,(\mathbf{P}_{\text{f}}, R_i) \\ \text{Ev}(\mathbf{P}_{\text{f}}, R_o) \end{bmatrix}. \tag{59}$$

The matrix $\mathbf{B}_{\text{f}}$ is identified from equations (54) and (58) and after modifications of the matrices $\mathbf{U}_0$ and $\mathbf{U}_1$ according to the polynomial degree of $\mathbf{P}_{\text{f}}$, equations (47), (48) and (50) apply equally for calculating the dynamic stiffness matrices.

3.2.3. *Fluid-filled pipe formulation*

The cylinder functional, $L_{cyl}$, is a function of the amplitudes of the cylinder displacements and their first and second $x$-derivatives, all these being functions only of $x$, so that it may be directly assembled. Before this, as proposed by Gavric [15], to achieve real valued matrices (in the absence of losses) and symmetric matrices (any losses), the variational parameters are chosen as

$$-\mathrm{i}u = u_1, v, w, \qquad \mathrm{i}u^a = u_1^a, v^a \text{ and } w^a. \tag{60}$$

Upon this being done, the Euler-Lagrange equations corresponding to the assembled functional $L$, equation (28), are

$$\mathbf{K_4}\,\partial^4\mathbf{U}/\partial\mathbf{x}^4 + \mathbf{K_2}\,\partial^2\mathbf{U}/\partial\mathbf{x}^2 + \mathbf{K_1}\partial\mathbf{U}/\partial\mathbf{x} + \mathbf{K_0}\mathbf{U} + \omega\mathbf{K_B}\mathbf{U} - \omega^2\mathbf{M}\mathbf{U} = \mathbf{0}, \tag{61}$$

where the matrices are detailed in the Appendix and where

$$\mathbf{U} = [u_1, v, w, \psi_1, \psi_2, \ldots, \psi_{N-3}]^{\mathrm{T}}. \tag{62}$$

$\psi_i$ are the $N$-3-d.o.f. in the fluid, as specified in the element formulations.

The set of ODE's, (61), have constant coefficients, so the solutions are of the form $\mathrm{e}^{\mathrm{i}\lambda x}$. Upon assuming this, the equations are, as in reference [17], transformed into a standard linear eigenvalue problem:

$$[\mathbf{A} - \lambda\mathbf{I}]\mathbf{X} = \mathbf{0}. \tag{63}$$

Hence, the solutions of equation (61) are

$$\mathbf{U} = \mathbf{X_m}\mathrm{e}^{\mathrm{i}\lambda_m x} \tag{64}$$

where $\lambda_m$ is any of the $2(N+1)$ eigenvalues and where $\mathbf{X_m}$ contains the $N$ appropriate elements of the corresponding eigenvector as detailed in reference [17].

### 3.3. NUMERICAL ACCURACY OF THE FE METHOD

To assess the numerical accuracy of the FE method presented in calculating wavenumbers in fluid-filled pipes, comparisons are made with results achieved with the exact formulation of Fuller and Fahy [13], here amended with the terms needed to be compatible with the Arnold and Warburton theory for cylinders [23, equation (2.9b)]. As good routines for complex valued Bessel functions are hard to find, e.g., in mathematical packages such as Maple and Matlab, the comparison is restricted to real-valued wavenumbers, corresponding to propagating waves in loss-less pipes.

The approach used in reference [13], namely solving the characteristic equation, once the sound pressure is expressed as a linear function of the radial displacement, results in a non-linear eigenvalue problem which here is solved by a standard routine in Matlab. Sometimes it is hard to get convergence of the solutions, even with starting approximations good to at least four digits accuracy. As the dispersion curves should be reasonably smooth functions of frequency, the values, shown in the figures below, when the routines converge to another solution are considered as outliers. No effort has been made to improve the routines for solving the non-linear eigenvalue problem. Even so, the problems encountered demonstrate the advantages of the FE method, resulting in a stable standard linear eigenvalue problem. Also, as implemented, when using one six-d.o.f. element for the fluid, the calculation time is hundreds, if not thousands, times smaller.

TABLE 1

*Geometrical and material parameters*

| Material | Poisson's ratio ($v$) | Density $\rho$ (kg/m$^3$) | Free wave speed $\sqrt{E/\rho}$, $c_f$ (m/s) |
|---|---|---|---|
| Steel | 0·3 | 7800 | 5196 |
| Water | – | 1000 | 1500 |
| Air | – | 1·3 | 340 |

Shell thickness 6 mm; shell radius 300 mm.

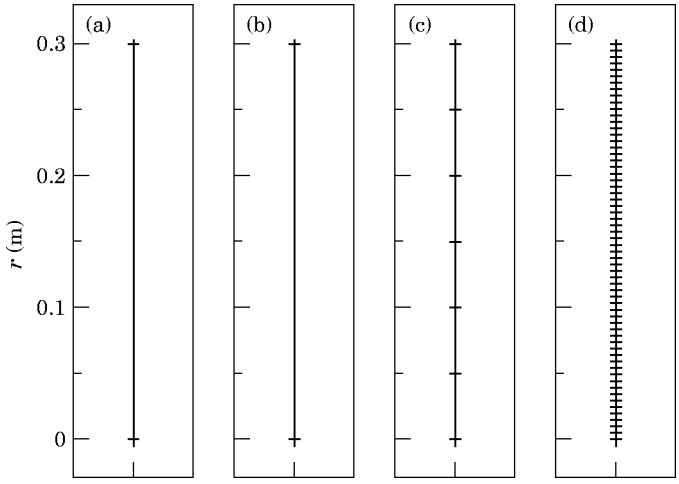


Figure 3. FE mesh used in the calculations. (a), six-d.o.f element; (b), standard FE, 1 element; (c), standard FE, 6 elements; (d), standard FE, 60 elements; +, node.

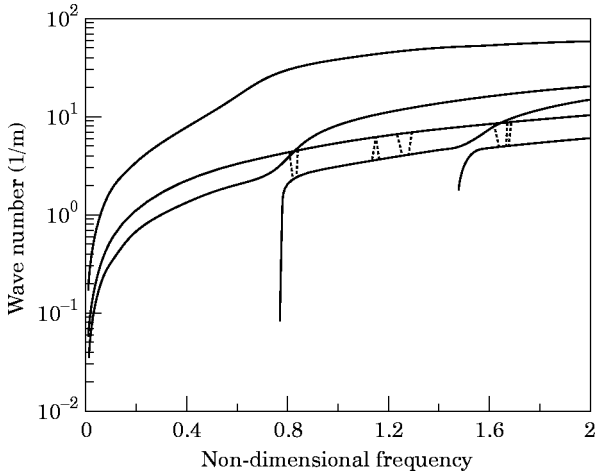


Figure 4. Propagating wavenumbers for $n = 0$; ——, FE method with one six-d.o.f. element; · · · ·, exact solution (only visible at the outliers).

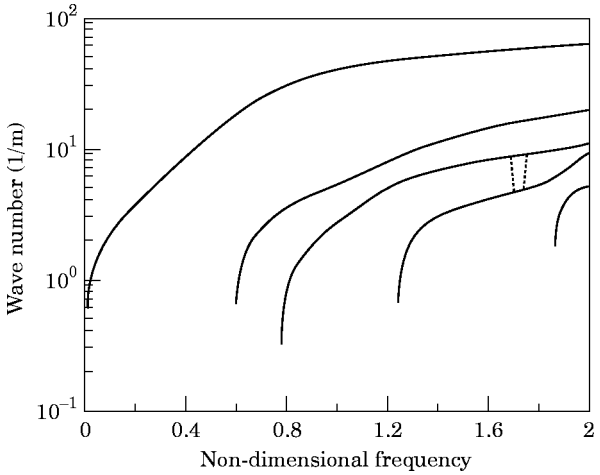


Figure 5. As Figure 3 but $n = 1$.

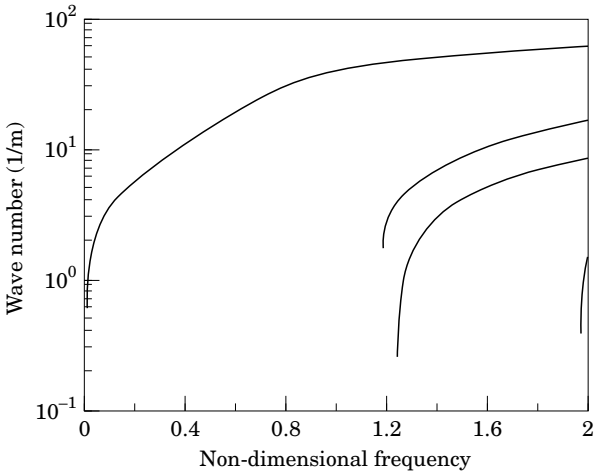


Figure 6. As Figure 3 but $n = 2$.

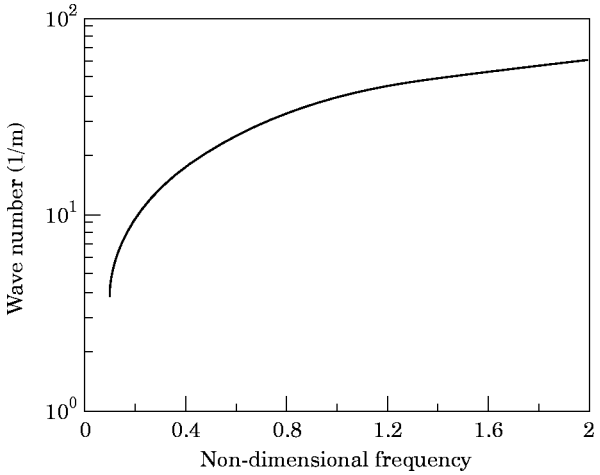


Figure 7. As Figure 3 but $n = 5$.

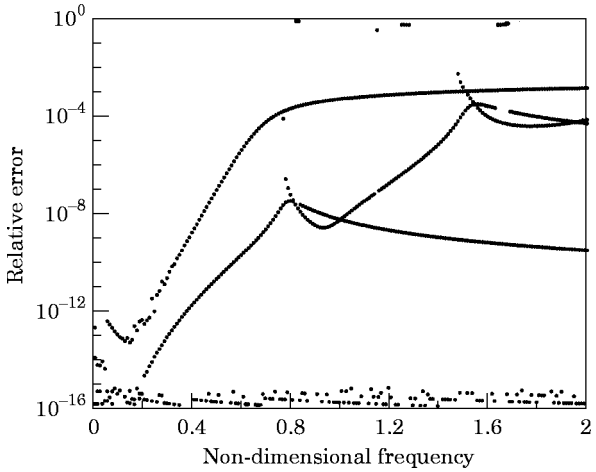


Figure 8. Relative errors in wavenumbers for $n = 0$; FE method with one six-d.o.f. element compared to exact solution; notably, the dots at the very top of the figure are considered as outliers—see text.

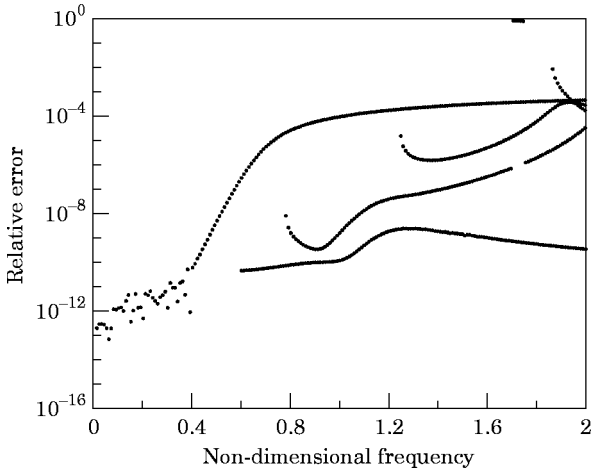


Figure 9. As figure 8 but for $n = 1$.

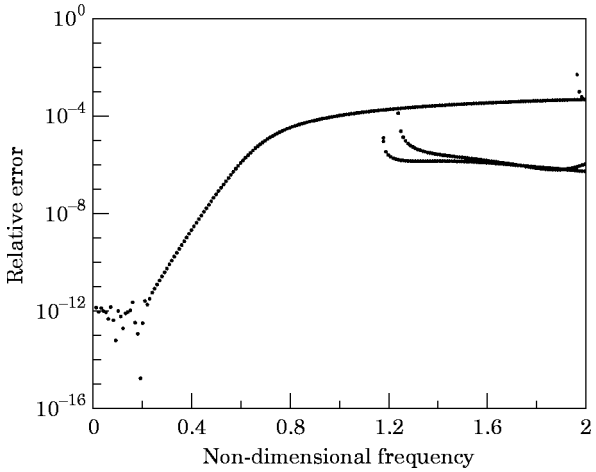


Figure 10. As figure 8 but for $n = 2$.

3.3.1. *Water-filled pipe*

The dispersion relations are solved for a loss-less water-filled steel pipe, with a trigonometric dependence: $n = 0$, 1, 2 or 5. The data used are found in Table 1 and the FE mesh is shown in Figure 3(a). The results below are shown as functions of non-dimensional frequency: $\textit{frequency}/\textit{ring frequency} = 2\pi Rf/\sqrt{E'/\rho}$. In Figures 4–7 are the real-valued wavenumbers, calculated with the exact method and the FE method with one six-d.o.f. element for the fluid. In Figures 8–11 are shown the relative differences between the solutions. Notably, for $n = 0$, as the torsional motion of the cylinder is uncoupled from the fluid motion, the relative difference is of the order of the digital noise in the computer. Near the cut-on frequencies the relative errors increases. This is anticipated, as by definition, the wavenumber is zero at cut-on, hence, if there is any error, the relative error is very large. Besides the outliers discussed above and, perhaps, at the cut-on frequencies, it is seen that for frequencies up to well above the ring frequency (2·8 kHz), the relative errors are less than $10^{-2}$, decreasing with higher order $n$, while being very much smaller at lower frequencies.

The accuracy of the FE method when using standard linear shape functions is displayed in Figures 12–14, where, for $n = 1$, the relative errors in calculations, for 1, 6 and 60 elements in the fluid, are shown. The FE-meshes used are shown in Figures 3(b–d). For frequencies up to approximately one third of the ring frequency, the single element solution is quite good; the six element model may be used at somewhat higher frequencies. For frequencies up to the ring frequency, the 60 element model is good while not quite as good as the single six-d.o.f. element model, though performing better at even higher frequencies.

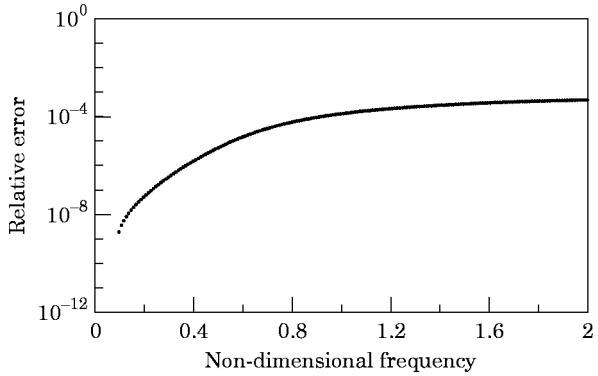


Figure 11. As figure 8 but for $n = 5$.

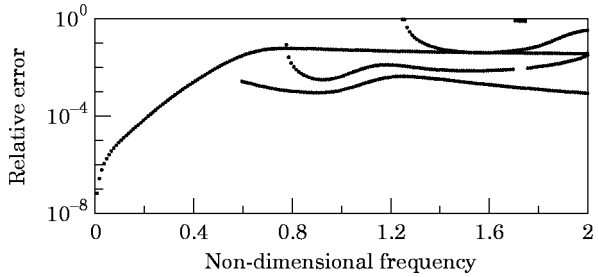


Figure 12. Relative errors in wavenumbers for $n = 1$; FE method with one standard two-d.o.f. element compared to exact solution.

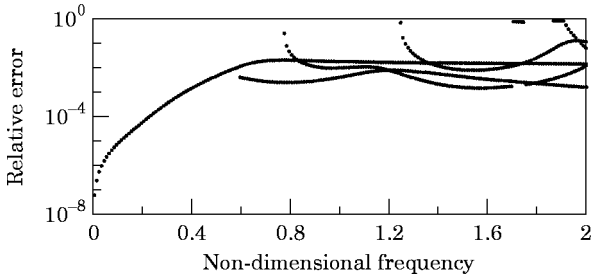


Figure 13. As Figure 12 but 6 elements.

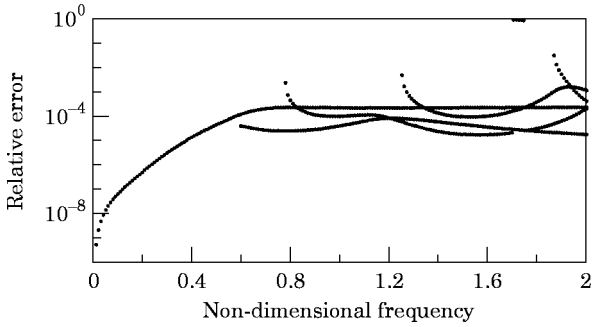


Figure 14. As Figure 12 but 60 elements.

### 3.3.2. *Mode shapes*

Mode shapes for propagating waves in a water filled steel pipe (data as in Table 1) are calculated by using the exact formulation [13] and a polynomial trial function with six-d.o.f.. For $n = 2$ at frequency $\Omega = 2$, there are four waves that may propagate; see Figure 6. In Figure 15 the radial displacements of the fluid are shown, normalized with the radial displacement of the cylinder so that the exact value at $r = 0{\cdot}3$ is unity. The mode

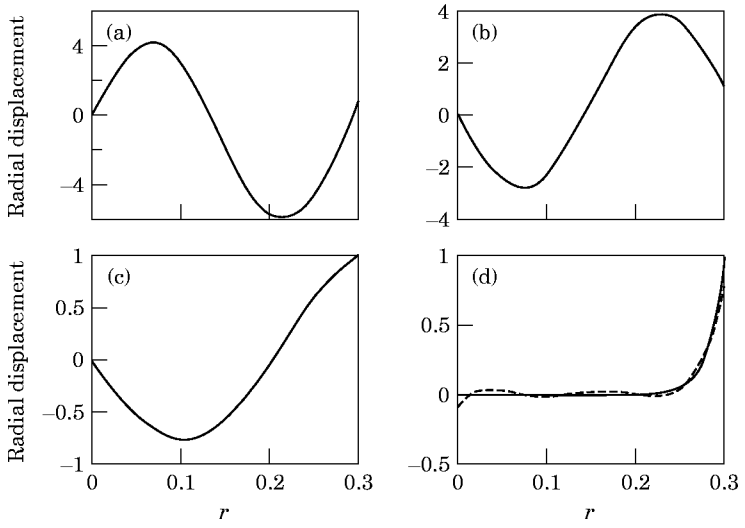


Figure 15. Radial fluid displacements for propagating modes, $n = 2$, $\Omega = 2$; (a), (b), (c), (d), modes with axial wavenumber in increasing order; ——, exact solution [13]; – – –, spectral FE with polynomial of sixth-order (only visible when different).

with the highest fluid wavenumber, Figure 15(a), is the one with the lowest axial wavenumber. This mode is just above cut-on; see Figure 6. Similarly, the mode with the sharp decay away from the pipe-wall, Figure 15(d), is the one which has the highest axial wavenumber and which is cut-on at a very low frequency. The mode shape for this mode

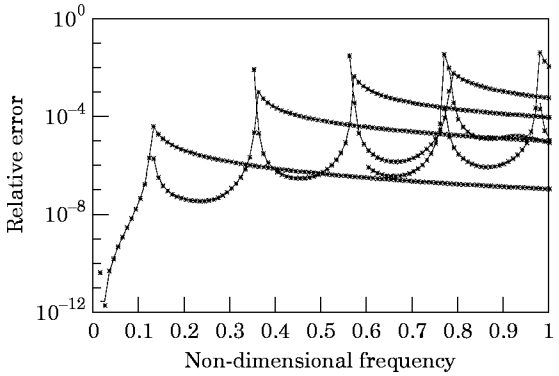


Figure 16. Two estimates of the relative errors in wavenumbers in an air filled pipe when using 100 standard two-d.o.f. elements; ——, $\varepsilon_1$; *, $\varepsilon_2$.

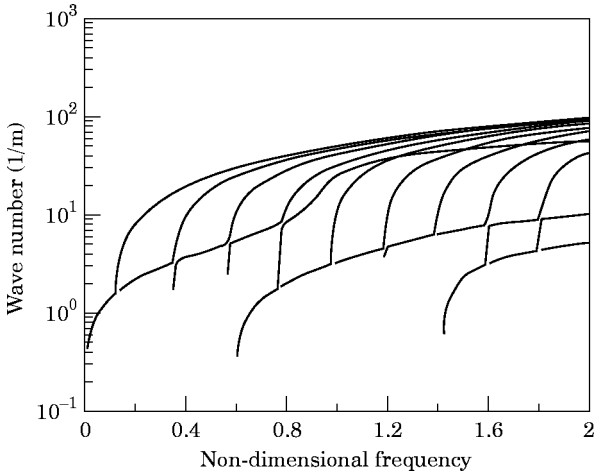


Figure 17. Wavenumbers in an air filled pipe, $n = 1$.

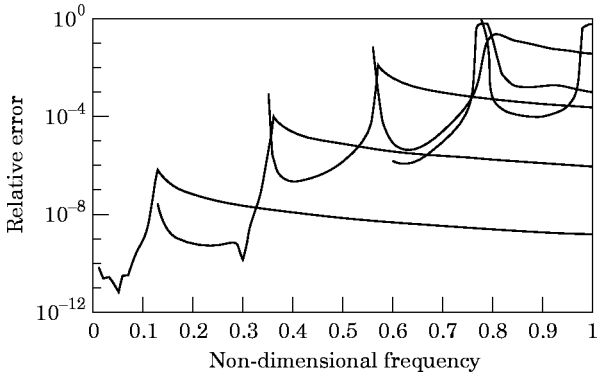


Figure 18. Estimated relative error of wavenumbers in an air filled pipe when using one six-d.o.f element: $\varepsilon_{6d}$.

is not accurately calculated. This is not surprising as the length scale is very short; the fluid wavenumber is imaginary and its amplitude is large: $|k_f R| \approx 19$. For this mode, the fluid loading on the cylinder is of an inertia character. Apparently, see Figure 10, even though the mode shape is not captured so well, the fluid loading is calculated sufficiently accurately.

The ability of the higher order polynomial shape functions to adapt to different displacement fields is one of the major advantages. When using standard linear shape functions, for the mode in Figure 15(d) a very fine mesh near the pipe-wall is needed whereas for the other modes the nodes should be uniformly distributed. Thus, if the same model is used, in either case there will be redundant d.o.f.. The higher order polynomial shape functions, however, in both cases use all of their ability to model the motion.

For standard FE there are rules of thumb for the mesh size, e.g., when using cubic shape functions for a beam there should be approximately six elements per wavelength. For higher order polynomial shape functions, the similar rule is that the number of half-wavelengths in the trial function with the shortest wavelength should be at least as many as in the true solution [19]. Hence, with a polynomial of degree six, it should be possible to model two or three half-wavelengths [19, Table 1]. Some numerical experiments have been made, with the six-d.o.f. element derived in section 3.2, confirming this rule of thumb. With this element, very good accuracy results if there is one wavelength per element; quite good accuracy results if there is one and a half wavelength, while if there are two wavelengths, the results are inaccurate. Similarly, when there is an exponential decay, as in Figure 15(d), results are good if $|k_f R| \leqslant 9$ while, as in the figure, when the 'wavenumber' is twice as big, results are poor. With higher order polynomial shape functions, the transmission from good results to poor results is rather abrupt.

### 3.3.3. *Air-filled pipe*

The dispersion curves for the same pipe, filled with air, are calculated for $n = 1$, with the preferred single six-d.o.f. element used for the fluid. In this case, the routines for solving the non-linear eigenvalue problem did not converge properly; hence other means were used to establish the accuracy of the FE method. For standard, piece-wise linear, finite elements applied to a second order equation, it is well known [12] that the errors are proportional to the square of the element size. Hence, increasing the number of elements by a factor $\sqrt{2}$ reduces the errors by half. To establish this, calculations were made with 50, 71 and 100 standard finite elements. Then, it is believed

$$Wa_{50} \approx Wa(1 + 4\varepsilon), \qquad Wa_{71} \approx Wa(1 + 2\varepsilon), \qquad Wa_{100} \approx Wa(1 + \varepsilon), \tag{65}$$

where $Wa_{50}$ is a wavenumber calculated with 50 elements, $Wa$ is the correct wavenumber and $\varepsilon$ is an estimate of the relative errors resulting from the 100 element calculation. In Figure 16, two estimates of $\varepsilon$, namely

$$\varepsilon_1 = |Wa_{100} - Wa_{71}|/Wa_{100}, \qquad \varepsilon_2 = |Wa_{71} - Wa_{50}|/2Wa_{100}, \tag{66}$$

are plotted, showing the assumption to be approximately true. Then, applying a Richardson extrapolation [26, section 7.2.2] reduces the errors considerably. Thus, the improved estimate of the wavenumbers, shown in Figure 17, is

$$Wa_{imp} = 2Wa_{100} - Wa_{71}. \tag{67}$$

With this estimate used as a reference, an on-the-average conservative estimate of the relative errors resulting when using the single six-d.o.f. element, shown in Figure 18, is

$$\varepsilon_{6d} = |Wa_{imp} - Wa_{6d}|/Wa_{imp}, \tag{68}$$

where $Wa_{6d}$ are the wavenumbers calculated with the six-d.o.f. element. From Figure 18 it is concluded that for an air-filled pipe the single six-d.o.f. element could be used for frequencies up to well above a third of the ring frequency: that is, for a pipe with 600 mm diameter up to approximately 1 kHz and for a pipe with 100 mm diameter up to 6 kHz.

## 4. SPECTRAL FINITE ELEMENT FORMULATION

For a beam element, it is possible to design an Exact Spectral Finite Element; "Exact" indicating that base functions are chosen as the local solutions of the governing, source free, equations of motions [6]. The basic steps are, as demonstrated in reference [7]: (1) formulate a bi-linear functional expressing the "virtual work" on the true element and on an adjoint element; (2) assume cross-sectional displacements, expressed as linear functions of displacements on the elements axis (or as functions of any other convenient variational parameters); (3) derive equations of motion by varying these 'displacements'; (4) calculate the base functions from the linear eigenvalue problem resulting, when solutions to the equations of motion with an exponential spatial dependence are sought for; (5) calculate trial functions, by standard matrix algebra, as linear combinations of the base functions having an explicit dependence of the nodal displacements, i.e., the displacements at the beam ends; (6) calculate the local dynamic stiffness matrix, utilizing the exact expressions for derivatives of exponential functions and of integrals of products of such functions; these calculations, avoiding numerical quadrature, result in expressions that are easily performed by standard matrix algebra.

Whereas in reference [7] the beam cross-sectional displacements were assumed according to the Navier hypothesis, here, in section 3, the cross-sectional displacements were found by a trigonometric decomposition and a polynomial assumption. Upon this basis, steps (3) and (4) were performed, producing equation (64) as the solutions of the equations of motion. These solutions are used below as base functions in a spectral finite element formulation for a straight fluid filled pipe. Also, FE formulations for rigid masses and flanges attached to straight pipes are derived.

### 4.1. FLUID FILLED PIPES

The essential boundary conditions for a finite element based on the functional $L$, equation (28), are the displacements $u$, $v$, $w$, the rotational displacement of the cylinder wall $\partial w/\partial x$ and the value of the velocity potential, $\psi(r)$, on the cross-section. If the pipe is joined to a similar pipe or if the fluid obeys a pressure release or blocked displacement boundary condition, the boundary conditions for the velocity potential could equally be expressed as conditions on $\Psi$, the variational parameters used in the fluid formulations in Section 3.2.

With this assumed, a trial function for a straight fluid filled pipe, which is a solution to its equations of motion and which depends linearly on its nodal values of displacements and velocity potential at the ends, is

$$\begin{bmatrix} u \\ v \\ w \\ \psi \end{bmatrix} = \begin{bmatrix} \cos n\phi\, \mathbf{B_u} \\ \sin n\phi\, \mathbf{B_v} \\ \cos n\phi\, \mathbf{B_w} \\ \cos n\phi\, \mathbf{P_f}(r) * \mathbf{B_f} * \mathbf{B_F} \end{bmatrix} * \operatorname{diag}(\exp(\boldsymbol{\alpha} x - \boldsymbol{\alpha}_p L)) * \mathbf{A} * \begin{bmatrix} \mathbf{V_1} \\ \mathbf{V_2} \end{bmatrix}, \quad (69)$$

where $\mathbf{P_f}$ and $\mathbf{B_f}$ are defined in section 3.2, the $2N+2$ length row vectors $\boldsymbol{\alpha}$, $\boldsymbol{\alpha}_p$, $\mathbf{B_u}$, $\mathbf{B_w}$ are

$$\alpha[m] = i\lambda_{\mathbf{m}},\ \boldsymbol{\alpha}_p[m] = \begin{Bmatrix} \boldsymbol{\alpha}[m], & \mathrm{Re}\,(\boldsymbol{\alpha}[m]) \geqslant 0 \\ -\boldsymbol{\alpha}[m], & \mathrm{Re}\,(\boldsymbol{\alpha}[m]) < 0 \end{Bmatrix}$$

$$\mathbf{B_u}[m] = i\mathbf{X_m}[1],\ \mathbf{B_v}[m] = \mathbf{X_m}[2],\ \mathbf{B_w}[m] = \mathbf{X_m}[3], \tag{70}$$

while the $(N-3) * (2N+2)$ matrix $\mathbf{B_F}$ has elements

$$\mathbf{B_F}[q, m] = \mathbf{X_m}[3+q], \tag{71}$$

where $\lambda_{\mathbf{m}}$ and $\mathbf{X_m}$ are the eigenvalues and eigenvectors found from the dispersion relations. These are defined in equation (64).

The vectors $\mathbf{V_1}$, $\mathbf{V_2}$ contain the nodal displacements, $u$, $v$, $w$, $-\partial w/\partial x$ and $\Psi$ at the two ends. If these ends are at $x = \pm L$, the $(2N+2) * (2N+2)$ matrix $\mathbf{A}$ is governed by boundary conditions

$$\begin{bmatrix} \begin{bmatrix} \mathbf{B_u} \\ \mathbf{B_v} \\ \mathbf{B_w} \\ -\boldsymbol{\alpha} \cdot{}^* \mathbf{B_w} \\ \mathbf{B_f} * \mathbf{B_F} \end{bmatrix} * \mathrm{diag}(\exp(-\boldsymbol{\alpha}L - \boldsymbol{\alpha}_p L)) \\ \begin{bmatrix} \mathbf{B_u} \\ \mathbf{B_v} \\ \mathbf{B_w} \\ -\boldsymbol{\alpha} \cdot{}^* \mathbf{B_w} \\ \mathbf{B_f} * \mathbf{B_F} \end{bmatrix} * \mathrm{diag}(\exp(\boldsymbol{\alpha}L - \boldsymbol{\alpha}_p L)) \end{bmatrix} * \mathbf{A} * \begin{bmatrix} \mathbf{V_1} \\ \mathbf{V_2} \end{bmatrix} = \mathbf{I} * \begin{bmatrix} \mathbf{V_1} \\ \mathbf{V_2} \end{bmatrix}. \tag{72}$$

The scaling of the base functions used in equations (69) and (72), and originally introduced in reference [7], results in the exponential functions having magnitudes that are unity at one end, then decreasing exponentially towards the other end. For cylinders, this scaling is necessary as the near field terms, especially those corresponding to the standing decaying waves [13], have wavenumbers with large real parts. With this scaling, the results in [7] indicate that the formulation presented here could be used for arbitrarily long cylinders without any numerical difficulties, except for extremely short cylinders (for which anyway the Arnold and Warburton cylinder theory is not valid [23]).

Because of the symmetry of the original equations, the adjoint system's displacements are as those of the true system, i.e., as in equation (69), except that they are functions of the adjoint systems nodal displacements. By inserting the displacements into the functional $L$ it is calculated, as in reference [7] that

$$L = [\mathbf{V_1^{a^T}} \quad \mathbf{V_2^{a^T}}] * \mathbf{Lag_{pipe}} * \begin{bmatrix} \mathbf{V_1} \\ \mathbf{V_2} \end{bmatrix}, \tag{73}$$

where the dynamic stiffness matrix $\mathbf{Lag}_{\text{pipe}}$ is

$$\begin{aligned}\mathbf{Lag}_{\mathbf{pipe}} = \mathbf{E\_Is}(\boldsymbol{\alpha}, L) \cdot^{*} [&E' T_c R \Lambda_n (\boldsymbol{\varepsilon}_x^{\mathrm{T}} \boldsymbol{\varepsilon}_x + \boldsymbol{\varepsilon}_\phi^{\mathrm{T}} \boldsymbol{\varepsilon}_\phi + \nu(\boldsymbol{\varepsilon}_x^{\mathrm{T}} \boldsymbol{\varepsilon}_\phi + \boldsymbol{\varepsilon}_\phi^{\mathrm{T}} \boldsymbol{\varepsilon}_x)\\ &+ g \boldsymbol{\gamma}^{\mathrm{T}} \boldsymbol{\gamma} + (T_c^2/12)(\boldsymbol{\kappa}_1^{\mathrm{T}} \boldsymbol{\kappa}_1 + \boldsymbol{\kappa}_2^{\mathrm{T}} \boldsymbol{\kappa}_2 + \nu(\boldsymbol{\kappa}_1^{\mathrm{T}} \boldsymbol{\kappa}_2 + \boldsymbol{\kappa}_2^{\mathrm{T}} \boldsymbol{\kappa}_1) + g \boldsymbol{\tau}^{\mathrm{T}} \boldsymbol{\tau})\\ &- \omega^2/c_L^2 (\mathbf{B}_{\mathbf{u}}^{\mathrm{T}} \mathbf{B}_{\mathbf{u}} + \mathbf{B}_{\mathbf{v}}^{\mathrm{T}} \mathbf{B}_{\mathbf{v}} + \mathbf{B}_{\mathbf{w}}^{\mathrm{T}} \mathbf{B}_{\mathbf{w}}))\\ &+ \mathbf{B}_{\mathbf{F}}^{\mathrm{T}} * [\mathbf{k_0} - \omega^2 \mathbf{m}] * \mathbf{B}_{\mathbf{F}} + \mathrm{diag}(\boldsymbol{\alpha}) * \mathbf{B}_{\mathbf{F}}^{\mathrm{T}} * \mathbf{k_2} * \mathbf{B}_{\mathbf{F}} * \mathrm{diag}\,(\boldsymbol{\alpha})\\ &- \omega (\mathbf{B}_{\mathbf{w}}^{\mathrm{T}} * \mathbf{C} * \mathbf{B}_{\mathbf{F}} + \mathbf{B}_{\mathbf{F}}^{\mathrm{T}} * \mathbf{C}^{\mathrm{T}} * \mathbf{B}_{\mathbf{W}})], \end{aligned} \tag{74}$$

where the matrices $\mathbf{k_0}$, $\mathbf{m}$, $\mathbf{k_2}$ and the vector $\mathbf{C}$ are defined in equations (48) and (50) and where

$$\boldsymbol{\varepsilon}_x = \boldsymbol{\alpha} \cdot^{*} \mathbf{B}_{\mathrm{u}}, \qquad \boldsymbol{\varepsilon}_\phi = (n\mathbf{B}_{\mathrm{v}} + \mathbf{B}_{\mathrm{w}})/R, \qquad \boldsymbol{\gamma} = -n\mathbf{B}_{\mathrm{u}}/R + \boldsymbol{\alpha} \cdot^{*} \mathbf{B}_{\mathrm{v}},$$

$$\boldsymbol{\kappa}_1 = -\boldsymbol{\alpha} \cdot\hat{}\ 2 \cdot^{*} \mathbf{B}_{\mathrm{w}}, \qquad \boldsymbol{\kappa}_2 = (n\mathbf{B}_{\mathrm{v}} + n^2 \mathbf{B}_{\mathrm{w}})/R^2, \qquad \tau = 2/R(\boldsymbol{\alpha} \cdot^{*} \mathbf{B}_{\mathrm{v}} + n\boldsymbol{\alpha} \cdot^{*} \mathbf{B}_{\mathrm{w}}). \tag{75}$$

The matrix generating function $\mathbf{E\_Is}$ is defined in reference [7] as

$$\begin{aligned}\mathbf{E\_Is}(\boldsymbol{\alpha}, L) &= \int_{-L}^{L} \exp(\boldsymbol{\alpha} x - \boldsymbol{\alpha}_{\mathbf{p}} L)^{\mathrm{T}} * \exp(\boldsymbol{\alpha} x - \boldsymbol{\alpha}_{\mathbf{p}} L)\, \mathrm{d}x\\ &= (\exp\,(\boldsymbol{\alpha} L - \boldsymbol{\alpha}_{\mathbf{p}} L)^{\mathrm{T}} * \exp(\boldsymbol{\alpha} L - \boldsymbol{\alpha}_{\mathbf{p}} L)\\ &\quad - \exp(-\boldsymbol{\alpha} L + \boldsymbol{\alpha}_{\mathbf{p}} L)^{\mathrm{T}} * \exp(-\boldsymbol{\alpha} L - \boldsymbol{\alpha}_{\mathbf{p}} L)) \cdot/\mathbf{Al}\end{aligned}$$

where

$$\mathbf{Al}[i, j] = \boldsymbol{\alpha}[i] + \boldsymbol{\alpha}[j]. \tag{76}$$

The formulas above apply directly if the fluid is described by only one finite element. If instead, many elements are used to describe the fluid motion, $\mathbf{k_0}$, $\mathbf{k_2}$ and $\mathbf{m}$ are block diagonal matrices where for each element the corresponding block is calculated as in equation (48). Notably, when using one six-d.o.f. element for the fluid, the complete element formulation for an arbitrarily long pipe (that is, assembling the dispersion relations and solving these, as in section 3, and the evaluation of the dynamic stiffness matrix, equation (74)), requires only 0·2 s on a PC (586) with Matlab. When using a more efficient code and a more powerful computer, it should be substantially quicker.

### 4.2. FLANGES

The motion of the flanges are described by the functional $L_{fla}$, equation (13), with the displacements as in equation (10). The flanges are divided into cylindrical segments, $R_i \leqslant r \leqslant R_o$, in which a polynomial description of $u$, $v$ and $w$ are assumed with that for $u$ and $v$ compatible:

$$u(r) = \mathbf{P}_{\mathbf{u}}(r) * \mathbf{A}_{\mathbf{u}} * \mathbf{U}, \qquad v(r) = \mathbf{P}_{\mathbf{u}}(r) * \mathbf{A}_{\mathbf{v}} * \mathbf{U}, \qquad w(r) = \mathbf{P}_{\mathbf{w}}(r) * \mathbf{A}_{\mathbf{w}} * \mathbf{U}. \tag{77}$$

$\mathbf{U}$ contains the variational parameters which must include the values of $u$, $v$ and $w$ and $\partial w/\partial r$ at the boundaries. All other variational parameters in $\mathbf{U}$ must project on d.o.f. without any boundary displacements. On this basis, $\mathbf{A}_{\mathbf{u}}$, $\mathbf{A}_{\mathbf{v}}$ and $\mathbf{A}_{\mathbf{w}}$ are determined as in Section 3.2. Inserting the displacements into the functional $L_{fla}$, equation (13), yields

$$L_{fla} = \mathbf{U}^{\mathrm{T}} * \mathbf{Lag}_{\mathbf{fla}} * \mathbf{U}, \tag{78}$$

where, upon representing the polynomials $\mathbf{P_u}$, $\mathbf{P_u}/r$ with matrices $\mathbf{h_0}$, $\mathbf{h_2}$ and the polynomial $\mathbf{P_w}$ with matrix $\mathbf{k_0}$ and defining

$$\mathbf{h_1} = \text{Dif}\,(\mathbf{h}), \qquad \mathbf{I_{n,m}} = \text{Intr}\,(\mathbf{h_n}, \mathbf{h_m}, \mathbf{R}), \qquad \mathbf{R} = [R_i, R_o],$$

$$\mathbf{k_1} = \text{Dif}\,(\mathbf{k_0}, 2), \qquad \mathbf{k_2} = \text{Add}\left(\text{Mul}\left(\text{Dif}\,(\mathbf{k_0}), \begin{bmatrix} 1 \\ -1 \end{bmatrix}\right), \qquad \text{Mul}\left(\mathbf{k_0}, \begin{bmatrix} -n^2 \\ -2 \end{bmatrix}\right)\right),$$

$$\mathbf{k_3} = \text{Dif}\left(\text{Mul}\left(\mathbf{k_0}, \begin{bmatrix} -2n \\ -1 \end{bmatrix}\right)\right), \qquad \mathbf{J_{n,m}} = \text{Intr}\,(\mathbf{k_n}, \mathbf{k_m}, \mathbf{R}), \tag{79}$$

the dynamic stiffness matrix $\mathbf{Lag_{fla}}$ is found to be

$$\begin{aligned}\mathbf{Lag_{fla}} = {} & E' T_f \Lambda_n [\mathbf{A_u}^{\mathrm{T}} * \mathbf{I_{1.1}} * \mathbf{A_u} + [\mathbf{A_u} + n\mathbf{A_v}]^{\mathrm{T}} * \mathbf{I_{2.2}} * [\mathbf{A_u} + n\mathbf{A_v}] \\ & + \nu([\mathbf{A_u} + n\mathbf{A_v}]^{\mathrm{T}} * \mathbf{I_{2.1}} * \mathbf{A_u} + \mathbf{A_u}^{\mathrm{T}} * \mathbf{I_{1.2}} * [\mathbf{A_u} + n\mathbf{A_v}]) \\ & + g(\mathbf{A_v}^{\mathrm{T}} * \mathbf{I_{1.1}} * \mathbf{A_v} - [n\mathbf{A_u} + \mathbf{A_v}]^{\mathrm{T}} * \mathbf{I_{2.1}} * \mathbf{A_v} - \mathbf{A_v}^{\mathrm{T}} * \mathbf{I_{1.2}} * [n\mathbf{A_u} + \mathbf{A_v}] \\ & + [n\mathbf{A_u} + \mathbf{A_v}]^{\mathrm{T}} * \mathbf{I_{2.2}} * [n\mathbf{A_u} + \mathbf{A_v}]) \\ & + (T_f^2/12)\mathbf{A_w}^{\mathrm{T}} * [\mathbf{J_{1.1}} + \mathbf{J_{2.2}} + \nu(\mathbf{J_{1.2}} + \mathbf{J_{2.1}}) + g\mathbf{J_{3.3}}] * \mathbf{A_w} \\ & - \omega^2/c_L^2(\mathbf{A_u}^{\mathrm{T}} * \mathbf{I_{0.0}} * \mathbf{A_u} + \mathbf{A_v}^{\mathrm{T}} * \mathbf{I_{0.0}} * \mathbf{A_v} + \mathbf{A_w}^{\mathrm{T}} * \mathbf{J_{0.0}} * \mathbf{A_w})].\end{aligned} \tag{80}$$

### 4.3. RIGID MASS

The functional determining the 'virtual work' of a rigid mass is

$$L_{mass} = [\mathbf{U}^a]^{\mathrm{T}} * \mathbf{Lag_{mass}} * \mathbf{U}, \tag{81}$$

where $\mathbf{U} = [u\ v\ w\ \phi_x\ \phi_y\ \phi_z]^{\mathrm{T}}$ are the displacements at a local node at the mass centre, with respect to co-ordinate axes coincident with the principal axes. The dynamic stiffness matrix in this case is

$$\mathbf{Lag_{mass}} = -\omega^2\,\text{diag}\,(M \quad M \quad M \quad J_x \quad J_y \quad J_z), \tag{82}$$

where $M$ is the mass and $J_x$, $J_y$, $J_z$ are mass moments of inertia.

When the rigid mass is on a pipe, its inertia will result in forces that couple the waves in the pipe. Hence, if a pipe is modelled with several co-existing spectral finite elements, describing waves with different trigonometric dependence on $\phi$, these elements are coupled. The motion of a point on the cylinder is the sum of the motion of all trigonometric orders $n$, each being as in equation (69). So, with directions as in Figure 19, the motion is

$$u = \sum_{n=0}^{\infty} u_n \cos(n(\phi - \phi_0)), \qquad v = \sum_{n=0}^{\infty} v_n \sin(n(\phi - \phi_0)), \qquad w = \sum_{n=0}^{\infty} w_n \cos(n(\phi - \phi_0)),$$

$$\phi_x = \frac{1}{2}\left(\frac{1}{R}\frac{\partial u_z}{\partial \phi} - \frac{\partial u_\phi}{\partial z}\right) = \frac{1}{2R}\sum_{n=0}^{\infty} -(v_n + 2nw_n)\sin(n(\phi - \phi_0)),$$

$$\phi_y = \frac{1}{2}\left(\frac{\partial u_x}{\partial z} - \frac{\partial u_z}{\partial x}\right) = \sum_{n=0}^{\infty} -\frac{\partial w_n}{\partial x}\cos(n(\phi - \phi_0)), \qquad \phi_z = \frac{1}{2}\left(\frac{\partial u_y}{\partial x} - \frac{1}{R}\frac{\partial u_\phi}{\partial \phi}\right), \tag{83}$$

where $\phi_0$ represents the polarization of the element. Notably, for each trigonometric order, except for $n = 0$, in the general case there should be two elements with $\phi_0$ differing by $\pi/2$.

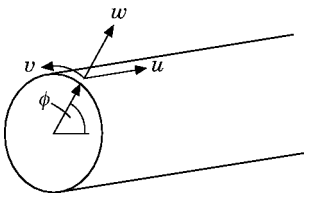


Figure 19. Displacements at a point on cylinder.

It is seen in the equations above that if the polarization of an incoming wave is $\phi_0 = 0$ then at $\phi = 0$ there are only displacements $u$, $w$ and $\phi_y$. Similarly, if $\phi_0 = \pi/2$ the only displacements are $v$, $\phi_x$ and $\phi_z$. With the mass above $\phi = 0$ and the principle axes of the mass in the $x$-, $y$-, and $z$- directions, these sets of displacements are uncoupled and may be treated separately.

The displacements $u$, $v$, $w$, $\phi_x$ and $\phi_y$ are thus expressed in terms of the nodal d.o.f. of the cylinder elements. Hence, the functional $L_{mass}$ is also expressed in the same terms and, by using the transformation [7, equation (117)] to account for the offset of the mass centre from the pipe-wall, its dynamic stiffness matrix is assembled to the global dynamic stiffness matrix.

The $\phi_z$ displacement, however, is more difficult to handle, as, with the $\partial u_y/\partial x$ term, it is not locally described but depends on the motion of the entire pipe. With the displacements as in equation (69), it is possible to describe the $\phi_z$ component as a function of the nodal displacements and the nodal displacements of the nearest cross section, on each side. This, however, leads to a rather complex element formulation, restricting the flexibility of the method. It is believed, although not demonstrated, that the most efficient formulation would instead result from using a small ring element, with cross-sectional displacements as in equation (69), but with a polynomial axial dependence.

If the rigid mass has a finite size, there is a spatial filtering of the waves with high order $n$, reducing the number of terms required in the summation (83). Also in the axial direction there is filtering, while, for a given $n$, the axial wavenumbers are always finite. The axial filtering is non-local and is positively best described by using the ring element proposed above.

If the rigid mass is at $-\alpha \leqslant \phi \leqslant \alpha$, the circular filtering results in motion as in equation (83), but with each term multiplied by the factor $\sin(n\alpha)/(n\alpha)$. This result is obtained when it is required that the average motion of the pipe should equal the motion of the rigid body. This may, of course, be only approximately true. Whereas it is perhaps more appropriate to impose this condition dynamically, by using Lagrange multipliers, it is believed that the errors when using the geometrically imposed restraints could be less than those resulting when a small and stiff object is treated as rigid.

Finally, it should be noted that the formulation and discussion above are not restricted to rigid masses. Any element could be similarly handled, provided it is connected to a point on the cylinder, or rigidly over a rectangular area, with the coupling being described by the six-displacement components. Thus, for example, any beam element or mass–spring system could be included in the model.

## 5. CALCULATION EXAMPLE

To demonstrate the spectral finite element formulations in the previous section, analysis of vibration of a simple pipe structure is presented. This example also reveals a mechanism that perhaps may cause failure due to fatigue.

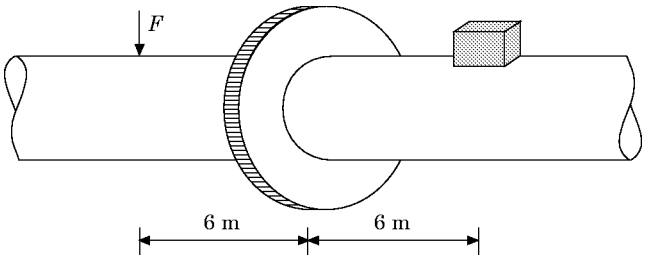


Figure 20. Investigated pipe structure.

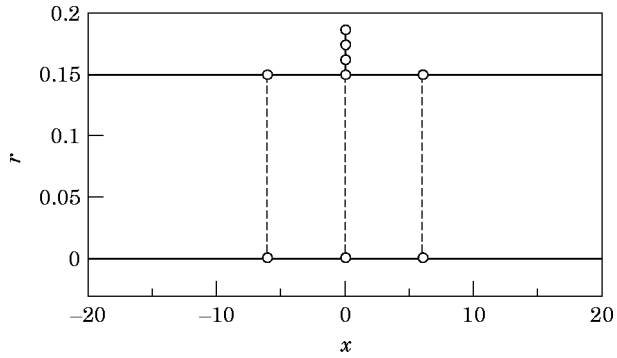


Figure 21. FE mesh used in the calculation example. Nodes joined by a dotted line belong to the same pipe-element; o, node. The nodes at $x = \pm 20 \times 10^6$ m are not shown.

TABLE 2

*Data used in the calculation example*

| | | | Lengths (km) | | | |
|---|---|---|---|---|---|---|
| Pipe | Radius (mm) | Thickness (mm) | | | | |
| | 150 | 2 | 20 000 | 0·006 | 0·006 | 20 000 |
| Flange | Thickness (mm) | Outer radius (mm) | Loss factor | Steel ($\eta_e$) | Water ($\eta_f$) | |
| | 10 | 75 | | 0·005 | 0·005 | |
| Mass | $L_x$(mm) | $L_y$(mm) | $L_z$(mm) | Mass (kg) | | |
| | 65 | 65 | 200 | 4 | | |
| | 100 | 100 | 126 | 10 | | |

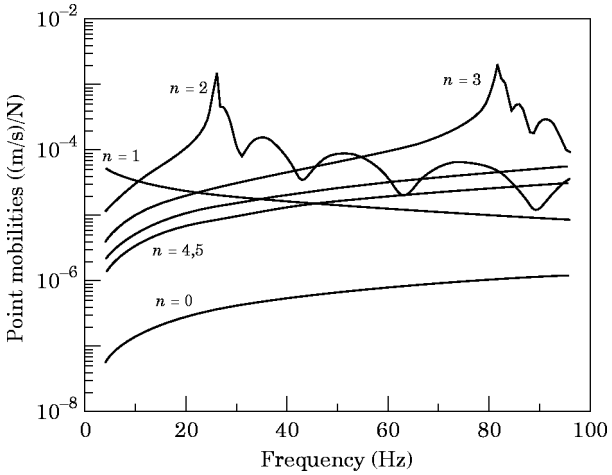


Figure 22. Mobility of a pipe structure for $n = 0$, 1, 2, 3, 4 and 5.

The structure investigated consists of two, very long, water-filled steel pipes, with a flange at their connection. The structure is defined in Figure 20 and the FE-mesh is shown in Figure 21. The material data are as in Table 1 with the loss factors and the geometry specified in Table 2. The element formulations are as in section 4. The flange is divided into three elements in which the in-plane motion is described with linear shape functions and out-of-plane motion with cubic functions. That is, the radial dependence of the flanges' displacements are described with standard thin-shell FE shape functions. The fluid motion is, for this low-frequency problem, described with three-term polynomials. Calculations are made with six terms in the trigonometric decomposition and the total calculation time, on a PC, with Matlab, is 5 seconds per frequency.

In Figure 22 the mobilities *radial velocity*/*radial force* are shown for each trigonometric order, $n = 0, 1, \ldots, 5$, at the point $x = -6$ m. The mobility for the $n = 0$ mode is low for all frequencies. At lower frequencies, the largest mobility is for the $n = 1$, beam mode. At cut-on of the shell modes, $n = 2$ (26 Hz) and $n = 3$ (82 Hz), the mobilities of these

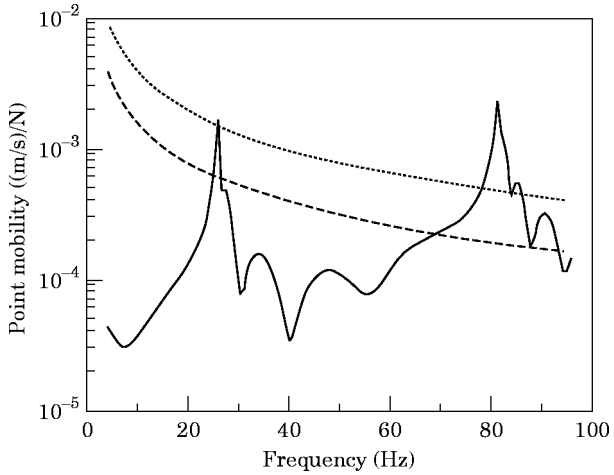


Figure 23. Point mobility of a pipe structure; ——, cylinder point mobility; – – –, point mobility for mass 10 kg; · · ·, point mobility for mass 4 kg.

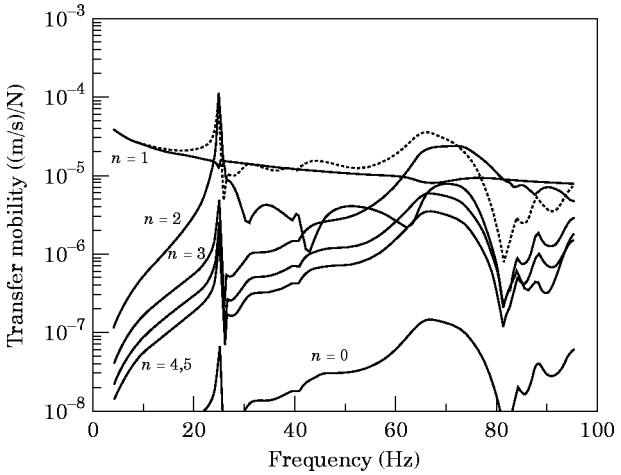


Figure 24. Transfer mobility of a pipe structure; ——, $n = 0$, 1, 2, 3, 4 and 5; · · ·, total transfer mobility.

modes are large. Just above cut-on, there are ripples in the mobilities caused by the reflections from the flange. Notably, this ripple is small for the beam mode. In Figure 23 the point mobility is shown, which is the sum of "all" ($n = 0, 1, \ldots, 5$) trigonometric orders. Also in Figure 23 are shown the point mobilities for rigid masses, 4 and 10 kg.

The pipe structure is excited on one side of the flange and the response on the other side is calculated. The excitation is only in the beam mode, thus imitating an arbitrary source far away in the structure so that all but the $n = 1$ mode have vanished due to reflections at restrictions such as flanges. In Figure 24 the responses at the rigid mass (10 kg) are shown for the different trigonometric orders. Whereas the response of the beam mode is almost as it would be if there was no mass, just below the cut-on frequencies, for the $n = 2$ and $n = 3$ modes, the response is high. As discussed in the previous section, the inertia force of the mass is a point force that excites all modes. Near cut-on, a mode's mobility is very large so that the total response is predominantly restricted by this mode's impedance. Below cut-on, this impedance is of stiffness character and may resonate with

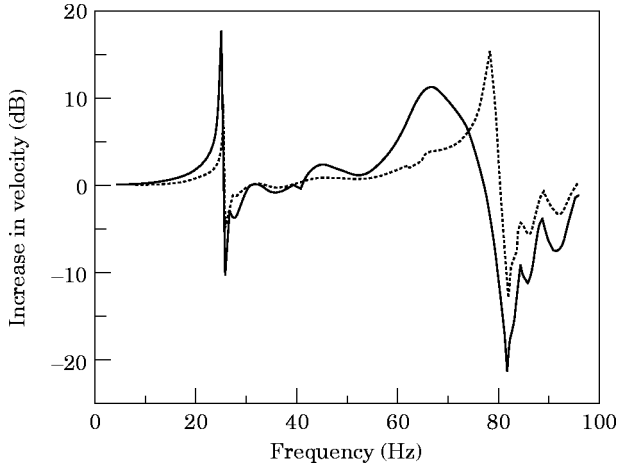


Figure 25. Increase in vibration velocity level when rigid mass is attached to pipe; ——, rigid mass 10 kg; · · · , rigid mass 4 kg.

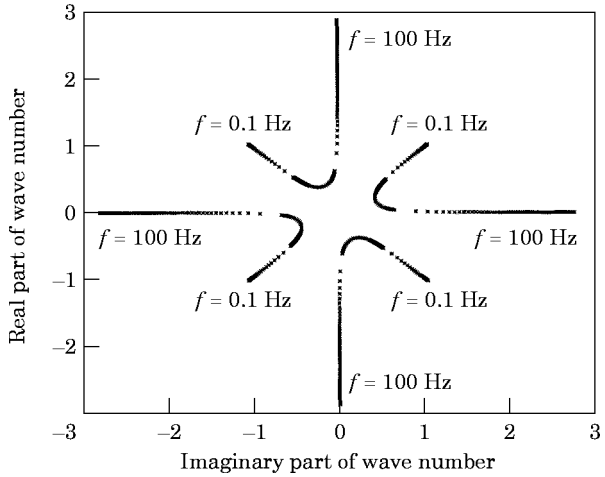


Figure 26. Phase plot of wavenumbers in water filled steel pipe for the $n = 2$ shell mode; lowest four solutions of the dispersion relations.

the mass's impedance. Also, below cut-on, there is no radiation damping for this mode, hence, at resonance, the response is predominantly restricted by the structural damping which, for a pipe structure, is often very small.

The total response of the pipe at the attachment point is calculated with masses of 4 kg and 10 kg, and, also without a mass. The increases in velocity level with the two masses are shown in Figure 25. Even though no attempt is made to match the mass and the pipe impedances, the velocity level is seen to increase by as much as 18 dB, when a mass is mounted on the pipe.

In Figure 26 is shown a phase plot of the wavenumbers for the $n = 2$, shell mode. Notably, the magnitudes of the wavenumbers are not zero at cut-on. This means that the axial stress, as well as the circumferential stress, could be large for the resonances discussed.

## 6. CONCLUSIONS

A spectral finite element formulation for the analysis of stationary vibration response in straight fluid filled pipes has been presented. In this finite element formulation, the base functions are the frequency dependent local solutions to the equations of motion. The formulation is valid for arbitrarily long pipes and losses may be distributed in the system and may vary with frequency.

In prismatic structures, the solutions of the equations of motion are expressed in terms of exponential functions, describing the propagation in the waveguide, together with corresponding cross-sectional mode shapes. The dispersion relations are found by using an FE discretization of the cross-sectional motion. To increase the numerical efficiency, methods for using FE shape functions with higher order polynomials have been developed. This reduces the required number of d.o.f. in the FE model by, roughly, a factor of the order of 10.

The numerical accuracy has been investigated by comparisons with results achieved with the exact formulation by Fuller and Fahy [13]. It is found that for a thin walled, water-filled steel pipe, and with only one finite element with a polynomial of sixth order, the accuracy is good for frequencies up to well above the cylinder ring frequency. For an air-filled steel pipe, the accuracy is similarly good, with only one FE, up to approximately one-third of the ring frequency. That is, for an air filled pipe with a diameter of 600 mm the accuracy is good up to approximately 1 kHz, this frequency increasing in inverse proportion to the diameter. Hence, many engineering problems can be solved by using only one, or a few, elements to describe the fluid.

The vibration response of a simple pipe structure consisting of an infinite pipe, a flange and a small rigid mass has been calculated. It is found that just below the cut-on of a shell mode, the stiffness controlled shell mode and the rigid mass may resonate, resulting in high vibration levels concentrated near the mass. It is believed that the stresses around the mass may become large, perhaps causing fatigue.

The major contribution of this work is considered to be the application of a modified Hamilton's principle describing non-conservative vibrations in the frequency domain. In this manner, the Gavric method [15] for calculating dispersion relations in wave guides is extended to cope with fluid elements and viscous motion. Also, the solutions to these dispersion relations are used in FE formulations. Finally, the approach has enabled the simultaneous use of dynamic stiffness methods and standard finite elements.

## ACKNOWLEDGMENTS

The financial support by TFR, Sweden and EPSRC, UK is gratefully acknowledged.

The author also acknowledges his sincerest gratitude to Professor Frank Fahy for enlightening discussions, for reading the manuscript and for suggesting improvements.

## REFERENCES

1. A. Wang and R. J. Pinnington 1990 *Proceedings of the Institute of Acoustics* **12**, 477–484. An impedance approach to pipework analysis using the transmission matrix method.
2. C. de Jong 1994 *Ph. D. Thesis Technisce Universiteit Eindhoven*. Analysis of pulsations and vibrations in fluid-filled pipe systems.
3. A. Frid 1989 *Journal of Sound and Vibration* **133**, 423–438. Fluid vibration in piping systems—a structural mechanics approach. Part 1: theory.
4. M. El-Raheb 1981 *Journal of the Acoustical Society of America* **71**, 296–306. Acoustic propagation in finite length elastic cylinders. Part 1: axisymmetric excitation.
5. M. El-Raheb and P. Wagner 1985 *Journal of the Acoustical Society of America* **78**, 738–746. Harmonic response of cylindrical and toroidal shells to an internal acoustic field. Part 1: theory.
6. I. Karasalo 1994 *Journal of Sound and Vibration* **172**, 671–688. Exact finite elements for wave propagation in range-independent media.
7. S. Finnveden 1994 *Acta Acustica* **2**, 461–482. Exact spectral finite element analysis of stationary vibrations in a railway car structure.
8. S. Finnveden 1996 *Acta Acustica* **82,** 478–497. Spectral finite element analysis of stationary vibrations in a beam-plate structure.
9. T. H. Richards and Y. T. Leung 1979 *Journal of Sound and Vibration* **55**, 363–376. An accurate method in structural vibration analysis.
10. R. Lunden and B. Åkesson 1983 *International Journal of Numerical Methods in Engineering* **19**, 431–449. Damped second order Rayleigh-Timoshenko beam vibration in space—an exact dynamic member stiffness matrix.
11. R. S. Langley 1990 *Journal of Sound and Vibration* **136**, 439–452. Analysis of power flow in beams and frameworks using the direct-dynamic stiffness method.
12. M. Petyt 1990 *Introduction to finite element vibration analysis*. Cambridge University Press.
13. C. R. Fuller and F. J. Fahy 1982 *Journal of Sound and Vibration* **81**, 501–518. Characteristics of wave propagation in cylindrical elastic shells filled with fluid.
14. G. Pavic 1990 *Journal of Sound and Vibration* **142**, 293–310. Vibrational energy flow in elastic cylindrical shells.
15. L. Gavric 1994 *Journal of Sound and Vibration* **173**, 113–124. Finite element computation of dispersion properties of thin-walled waveguides.
16. M. M. Ettouney, R. P. Daddazio and N. M. Abboud 1995 *Proceedings of the Third International Conference on Numerical Aspects of Wave Propagation Phenomena*. Scale independent elements for dynamic analysis of vibrating systems.
17. U. Orrenius and S. Finnveden 1996 *Journal of Sound and Vibration* **198,** 203–224. Calculation of wave propagation in rib-stiffened plate structure.
18. L. Meirovitch 1986 *Elements of Vibration Analysis*. New York: McGraw-Hill.
19. N. S. Bardell 1991 *Journal of Sound and Vibration* **151**, 263–289. Free vibrations of a flat plate using the hierarchical finite element method.
20. P. M. Morse and H. Feshbach 1953 *Methods of Theoretical Physics*. New York: McGraw-Hill.
21. G. M. L. Gladwell 1966 *Journal of Sound and Vibration* **4**, 172–186. A variational formulation for damped acousto-structural problems.
22. R. N. Arnold and G. B. Warburton 1949 *Proceedings of the Royal Society of London*, **A197**, 238–256. Flexural vibrations of the walls of thin cylindrical shells having freely supported ends.
23. A. W. Leissa 1973 *Vibrations of shells* (NASA SP-288). Washington DC: U.S. Government Printing Office.
24. A. D. Pierce 1989 *Acoustics*. Acoustical Society of America.
25. P. M. Morse and K. U. Ingard 1968 *Theoretical Acoustics*. New York: McGraw-Hill
26. G. Dahlquist, A. Björk and N. Anderson 1974 *Numerical Methods*. Englewood Cliffs, NJ: Prentice-Hall.

APPENDIX—*overleaf*

## APPENDIX

The matrices $\mathbf{K_4}$, $\mathbf{K_2}$, $\mathbf{K_1}$, $\mathbf{K_0}$, $\mathbf{K_b}$ and $\mathbf{M}$ in equation (61) are

$$\mathbf{K_4} = \begin{bmatrix} k_{\mathbf{4cyl}} & \mathbf{0} \\ \mathbf{0} & \mathbf{0} \end{bmatrix}, \qquad \mathbf{K_2} = -\begin{bmatrix} \mathbf{k_{2cyl}} & \mathbf{0} \\ \mathbf{0} & \mathbf{k_2} \end{bmatrix}, \qquad \mathbf{K_1} = -\mathbf{i}\begin{bmatrix} \mathbf{k_{1cyl}} & \mathbf{0} \\ \mathbf{0} & \mathbf{0} \end{bmatrix},$$

$$\mathbf{K_B} = -\begin{bmatrix} \mathbf{0} & \mathbf{C} \\ \mathbf{C}^{\mathrm{T}} & \mathbf{0} \end{bmatrix}, \qquad \mathbf{K_0} = \begin{bmatrix} \mathbf{k_{0cyl}} & \mathbf{0} \\ \mathbf{0} & \mathbf{k_0} \end{bmatrix}, \qquad \mathbf{M} = \begin{bmatrix} \mathbf{m_{cyl}} & \mathbf{0} \\ \mathbf{0} & \mathbf{m} \end{bmatrix},$$

where the matrices $\mathbf{k}_2$, $\mathbf{k}_0$, $\mathbf{m}$, describing the fluid are assembled with submatrices for each element as in equation (48). $\mathbf{C}$ is detailed in equation (50).

By using the Arnold and Warburton theory for cylinders, one finds

$$\mathbf{k_{4cyl}} = BR^3\begin{bmatrix} 0 & 0 & 0 \\ 0 & 0 & 0 \\ 0 & 0 & \beta \end{bmatrix},$$

$$\mathbf{k}_{2\mathrm{cyl}} = BR\begin{bmatrix} 1 & 0 & 0 \\ 0 & (1-\nu)/2 & 0 \\ 0 & 0 & 2n^2\beta \end{bmatrix} + \beta BR\begin{bmatrix} 0 & 0 & 0 \\ 0 & 2(1-\nu) & n(2-\nu) \\ 0 & n(2-\nu) & 0 \end{bmatrix},$$

$$\mathbf{k_{1cyl}} = B\begin{bmatrix} 0 & -n(1+\nu)/2 & -\nu \\ -n(1+\nu)/2 & 0 & 0 \\ -\nu & 0 & 0 \end{bmatrix},$$

$$\mathbf{k_{0cyl}} = \frac{B}{R}\begin{bmatrix} n^2(1-\nu)/2 & 0 & 0 \\ 0 & n^2 & n \\ 0 & n & 1+\beta n^4 \end{bmatrix} + \beta\frac{B}{R}\begin{bmatrix} 0 & 0 & 0 \\ 0 & n^2 & n^3 \\ 0 & n^3 & 0 \end{bmatrix},$$

$$\mathbf{m_{cyl}} = \rho T_c R \Lambda_n \begin{bmatrix} 1 & 0 & 0 \\ 0 & 1 & 0 \\ 0 & 0 & 1 \end{bmatrix},$$

where

$$B = \Lambda_n E T_c/(1-\nu^2), \qquad \beta = T_c^2/12R^2.$$